1987

Development of two-group, two-dimensional, frequency dependent detector adjoint function based on the nodal method

Soli T. Khericha
Iowa State University

Khericha, Soli T.

DEVELOPMENT OF TWO-GROUP, TWO-DIMENSIONAL, FREQUENCY DEPENDENT DETECTOR ADJOINT FUNCTION BASED ON THE NODAL METHOD

Iowa State University PH.D. 1987

PLEASE NOTE:

In all cases this material has been filmed in the best possible way from the available copy. Problems encountered with this document have been identified here with a check mark __✓__.

1. Glossy photographs or pages _____
2. Colored illustrations, paper or print _____
3. Photographs with dark background _____
4. Illustrations are poor copy _____
5. Pages with black marks, not original copy _____
6. Print shows through as there is text on both sides of page _____
7. Indistinct, broken or small print on several pages ✓
8. Print exceeds margin requirements _____
9. Tightly bound copy with print lost in spine _____
10. Computer printout pages with indistinct print _____
11. Page(s) _____ lacking when material received, and not available from school or author.
12. Page(s) _____ seem to be missing in numbering only as text follows.
13. Two pages numbered _____. Text follows.
14. Curling and wrinkled pages _____
15. Dissertation contains pages with print at a slant, filmed as received _____
16. Other _____

_____

_____

University
Microfilms
International

Development of two-group, two-dimensional, frequency dependent detector adjoint function based on the nodal method

by

Soli T. Khericha

A Dissertation Submitted to the
Graduate Faculty in Partial Fulfillment of the
Requirements for the Degree of
DOCTOR OF PHILOSOPHY
Major: Nuclear Engineering

Approved:

Signature was redacted for privacy.
In Charge of Major Work

Signature was redacted for privacy.
For the Major Department

Signature was redacted for privacy.
For the Graduate College

Iowa State University
Ames, Iowa

1987

TABLE OF CONTENTS

LIST OF TABLES

LIST OF FIGURES

page

DEDICATION

To

My Late Father

I. INTRODUCTION

It is common engineering knowledge that most mechanical structures are designed to tolerate some degree of vibration. The coolant flowing through the reactor can produce vibration in the core internals, control rods and fuel pins. Therefore, in a nuclear reactor, a large number of components are designed to withstand a tolerable degree of vibrational behavior, e.g., control rods in PWR are attached to the driving mechanism at the top and are free at the other end. Similarly, fuel pins are fixed at one end but are allowed clearance at the other end. However, this vibration, if excessive, can result in damage to the core.

From the safety point of view, excessive vibration causes a rather unique problem. It is difficult to apply conventional measuring techniques, i.e., displacement sensor/accelerometers on each component because of the hostile core environment and other instrumentation difficulties. The situation is aggravated by the fact that even normal vibration properties of the individual components cannot be investigated in mockup experiments since the same circumstances that prevent applications of conventional sensors, i.e. thermal and irradiation effects would change vibrational properties of the component as well.

Robinson (1) pointed out that the mechanical vibration of fuel elements or control rods is one major source of neutron noise, defined as fluctuation of the neutron flux about a mean value. Robinson also described a number of sources that affect the neutron density

fluctuations in a reactor. The inlet coolant temperature fluctuations also contribute to the neutron noise in a reactor (2). The fluctuation in the neutron flux density can be used to identify malfunctions, e.g., mechanical vibrations of reactor internals and provide an early warning to operators. In an operating power reactor there are many sources of noise acting simultaneously, thus making it difficult to extract meaningful information regarding a certain driving source without a full understanding of the fundamental interactions of each source with the neutron field. So far the properties of neutron noise have not been used effectively to identify the location of vibrating components.

Fluctuations of the neutron density due to an oscillating absorber rod have been demonstrated experimentally (1,3). In 1948, Weinberg and Schweinler (4) showed theoretically that oscillations of an absorber would lead to fluctuations of the neutron field in a pile. Further interest was generated in the mid '60s, when the effect of excessively vibrating control rods was identified in the neutron noise spectra of the Oak Ridge Research and High Flux Isotope reactors (1).

However; the problem of locating or estimating the position of a vibrating element and finding its amplitude of vibration is not completely solved at this time. It can be shown that a detector can be positioned to respond more effectively to noise sources located in a specific region of the core. A detector response model based on a space and frequency dependent detector adjoint function was developed

by H. Van Dam (5), and was shown to describe a detector "field of view." Using this model Pazsit (6), explained the basic interactions of the "global" and "local" components generated by a vibrating element. A "global" component is described as a reproduction of the coupled behavior of the neutron field caused by reactivity fluctuations produced by the vibrating element whereas a "local" component consists of the response as local flux fluctuation caused by its motion. The change in the global component through the space dependent transfer function is small in the frequency range below the break frequency. The local component depends very strongly upon the spatial location of the detector and vibrator and the type of motion. This spatial dependence of the local effect and its associated phase behavior can be used in establishing the location of the disturbance. The phase angle is defined as the ratio of the imaginary component to the real component of the detector adjoint function and can be obtained by solving the frequency dependent detector adjoint function.

The purpose of this research is to investigate the application of the nodal method to solve for the frequency dependent real and imaginary components of the detector adjoint functions. The basic techniques and the principles used in the nodalization method to calculate the static flux, as shown by A. Rohach (7,8) and M. Feiz (9), are used. The two-energy group frequency dependent detector adjoint functions presented by complex equations are expanded into real and imaginary parts as suggested by Van Dam (5) and are solved treating

them as standard four-energy group equations.

The method is based upon expansion of the flux in each node in polynomials. The reactor is divided into a number of large nodes. The flux and outgoing currents at each surface of the node are dependent on the average properties of the node and the incoming currents (10).

As a first step, a one-dimensional two-energy group model was developed. The phase angle and the magnitude of the detector adjoint function were calculated for a detector located in the middle of the south core tank of the Iowa State University UTR-10 reactor. Results were compared with the analytical solution developed by Al-Ammar (11).

Next, a two-dimensional one energy group model was developed. The phase angle and the magnitude of the detector adjoint function were calculated for the detector located in the center of a 200 cm x 200 cm homogenous subcritical reactor. The magnitude of the detector adjoint function was compared with the results from the EXTERMINATOR (12) computer code as well as the analytical solution (13). For this model, typical one-energy group cross sections from Duderstadt and Hamilton (14) were used.

In the third phase of the research, a two-dimensional two-energy group model was developed. Attempts to develop an analytical solution for a homogenous reactor as suggested by Weinberg and Schweinler (4) were not successful. A double sine series expansion using the classical Green's functions solution was developed. It was found that a large number of terms in the series were required for convergence,

and in some cases (near the source) convergence was not possible for even a very large number of terms. The result seems to follow the expected behavior of the Green's functions, however. Also, the phase angle varied within the expected range for the given frequency (15).

II. LITERATURE SURVEY

A vibrating control rod or other core component in the neutron field causes fluctuations in the neutron population commonly called neutron noise. This noise is interpreted in terms of the standard noise analysis functions; namely the auto power spectral density (ASPD), cross-power spectral density (CPSD), etc. The application of neutron noise analysis involves the interpretation of the fluctuating components of incore or excore neutron detector signals as an aid in identifying and locating the vibrating reactor core components. One of the early uses of neutron noise analysis was that described by Stephenson et al. (2). In 1966, Stephenson et al. (2) detected a peak in a neutron detector's power spectra caused by an excessively vibrating control rod. The peak disappeared when the faulty rod mechanism was replaced. A number of experiments have been carried out supporting the basic conclusion by Robinson (1) and Kosaly and Williams (16) among others, that changes in the reactor parameters cause the fluctuation in the neutron density.

An early and sophisticated treatment was given by Weinberg and Schweinler (4) in their classical paper about the theory of an oscillating absorber in a neutron field. The concept of a local and global component of the fluctuating flux was also presented in this paper. They showed that an absorber oscillating in a flux gradient at

a frequency below the periods of delayed neutrons or break frequency of the reactivity transfer function, produced both fluctuations in the flux fundamental mode, or global component, and fluctuations in the neutron field in the region nearby the absorber, or local component. They pointed out that the reactivity response varied at different frequencies of oscillation.

The frequency dependent response of a neutron detector to a vibrating neutron absorber was also demonstrated by Pazsit (17). He developed a one- and a two-group reactor model based on diffusion theory to demonstrate the spatial sensitivity of the response to detector and vibration source placement. Pazsit and Analytis (13) developed a two-dimensional reactor model to study the neutron noise generated by a vibrating absorber having two components of motion. Analytis (18) investigated the neutron noise resulting from fluctuations in the group constants with application to vibration and density perturbations.

Van Dam (5) extended the concept of the detector adjoint formulation to the frequency domain and provided a basis for modeling the response of a neutron detector to the fluctuations of core parameters. In this work, he also explained that in the plateau region of the reactor frequency response ($\lambda < \omega < \beta/\ell$), the detector adjoint function is approximately real.

Lee and Albrecht (19,20) studied the frequency response characteristic of the neutron field to a vibrating control rod. They developed the complex equations for a two-dimensional two-group

cylindrical model of a pressurized water reactor. They proposed a vibration localization technique based on the intersection of "detector response contours." To obtain the desired intersection, a scaling factor related to the rms amplitude of the vibration is used.

Pazsit and Glocker (21,22) investigated the localization problem for a vibrating control rod having two-dimensional periodic motion or stochastic motion. For the case of stochastic vibration an expression for the CPSD of the two components of motion was developed. They proposed a model to find an approximate location of the vibrating source by obtaining the intersection of roots of "localization equations" obtained using the measurements from three detectors. The model was based on a one-energy group, two-dimensional, bare, cylindrical reactor.

In addition to these investigations, extensive research work has been carried out at Iowa State University in the development of detector response models primarily based on the university's UTR-10 reactor. Huang and Danofsky (23) studied the changes in response of a neutron detector with separation distance from a noise source consisting of a small plexiglass container of water with air bubbling through it. They developed a three-dimensional two-energy group model for real detector adjoint functions. Good agreement was found between the model and the measurement.

Hennessy (24) developed a two-dimensional, two-energy group model of the reactor response to a moving neutron absorber using a Green's

function formulation. Experimental measurements supported the observed change in the ASPD of detector signals as a function of location relative to the vibration source, and supported the general results predicted by the model. In this work the detector response was assumed to be real.

Al-Ammar (11) and Al-Ammar and Danofsky (25) developed a complex two-energy group one-dimensional formulation of the detector adjoint system to study the effect of detector and vibrator location on the detector response. They placed a vibrating absorber in the center of the UTR-10 reactor and performed measurements to estimate the local and global components of the response of the moving detector. The vibration system used was limited in response due to flexing of the moving absorber rod. Borland (26) improved this system and further confirmed the global-local interpretation of the auto power spectral densities of the detector signal.

Sankoorikal (27) proposed a technique of localizing a vibration source based on the maximum likelihood function and confidence set estimation method. In this technique, the theoretical detector responses are combined with the measured detector responses to yield point estimates of vibrator position and intensity and confidence regions. In application, the amplitude characteristics are determined within an unknown scaling constant; however, the estimated relative amplitude of vibration can serve as a measure of change in the vibration amplitude in trending studies.

The EXTERMINATOR (12) code developed by Oak Ridge National Laboratory can be used to calculate the detector adjoint function at a particular location. However, a convergence problem was encountered when EXTERMINATOR was used to calculate the real and imaginary components of the detector adjoint function.

In general, the imaginary part of the detector adjoint function has been ignored on the basis that its magnitude is small compared to the real part in the plateau region of the reactor frequency response ($\lambda < \omega < \beta/\ell$) (5).

The purpose of this work is to investigate an application of a nodal technique to solve for the real and imaginary components of the detector adjoint function as a function of position in the core. As suggested by Van Dam (5), an N-neutron energy group diffusion equation formulation is expanded into 2N diffusion equations in the real and imaginary parts of the detector adjoint function. These equations are solved using the nodal technique. The nodal technique has been developed by A. Rohach (7,8) to perform multigroup one-dimensional and two-dimensional eigenvalue calculations. For this research, detector adjoint function and static flux calculations are limited to two-energy groups of neutron, i.e., fast and thermal. The nodal method is based upon expansion of the flux in terms of polynomials. In this technique a two-dimensional reactor is divided into a number of large nodes and the flux or the detector adjoint function in each node is expressed by a set of polynomials. The average flux and outgoing currents at each

surface of the node are functions of the properties within the volume and the current entering the node. The average flux and average net current on the interface are developed as continuous functions in the model.

III. DEVELOPMENT OF GREEN'S FUNCTION

A. General Formulation of Green's Function

In this section the frequency dependent detector adjoint equations are developed from the diffusion equations. The diffusion equations, including delayed neutrons, expressed in matrix form can be presented as follows:

$$L(\vec{r},E,t)\ \phi(\vec{r},E,t) = 0 \qquad 3.1$$

where

L = Space, energy and time dependent diffusion operator

ϕ = Flux and precursor vector

$\vec{r}$ = Space vector

t = Time domain

E = Neutron energy

As shown by Van Dam (5), introducing a perturbation δL in the diffusion operator in equation (3.1), canceling out the steady state terms and taking the Fourier Transform of the resulting equation, equation (3.1) transforms to the form

$$L(\vec{r},\omega)\delta\phi(\vec{r},\omega) = \delta L(\vec{r},\omega)\phi(\vec{r}) \qquad 3.2$$

where $\delta\phi(\vec{r},\omega)$ is the Fourier Transform of the fluctuation in the neutron flux due to a perturbation in the diffusion operator, and $\phi(\vec{r})$ is the steady state flux. The variable E, has been dropped for the purpose of this text as it has no impact on the derivation of the Green's function. In this work, perturbations are assumed to be in

only the absorption cross section. The term $\delta\phi\delta L$ will be very small compared to other terms in the equation and is assumed to be negligible.

From the definition of the adjoint operator, equation (3.2) yields

$$\langle L\delta\phi, \Psi \rangle = \langle \delta\phi, L^{+}\Psi \rangle \qquad 3.3$$

where

$$L^{+}(\vec{r},\omega)\Psi(\vec{r},\omega) = \Sigma_d(\vec{r},\omega) \qquad 3.4$$

Ψ is called the detector adjoint function and represents the field of view of a detector having the group cross sections Σ_d and L^{+} is the adjoint operator. Upon taking the inner product of Ψ with equation (3.2) and $\delta\phi$ with equation (3.4) and comparing the resultant equations with equation (3.3) yields

$$\langle \delta L(\vec{r},\omega)\phi(\vec{r}), \Psi(\vec{r},\omega) \rangle = \langle \delta\phi(\vec{r},\omega), \Sigma_d(\vec{r},\omega) \rangle \qquad 3.5a$$

The term on the right side in equation (3.5a) represents the response of a neutron detector to the fluctuations. Equation (3.5a), using the integral representation, can be written as

$$\int_{\vec{r}} [\delta L(\vec{r},\omega)\phi(\vec{r})]^{T}\Psi(\vec{r},\omega)d\vec{r} = \int_{\vec{r}} \delta\phi^{T}(\vec{r},\omega)\Sigma_d(\vec{r},\omega)d\vec{r} \qquad 3.5b$$

Equation (3.5b) is reduced to calculate the detector response, dR, to a perturbation located anywhere in the core as follows (11,13):

$$dR(\vec{r}_d,\vec{r}_p,\omega) = \gamma\left[\phi(\vec{r}_p)\left.\frac{\partial\Psi(\vec{r}_d,\vec{r},\omega)}{\partial\vec{r}}\right|_{\vec{r}=\vec{r}_p} + \Psi(\vec{r}_d,\vec{r}_p,\omega)\left.\frac{\partial\phi(\vec{r})}{\partial\vec{r}}\right|_{\vec{r}=\vec{r}_p}\right]\epsilon(\omega) \qquad 3.6$$

where

$$\epsilon(\omega) = \int_{-\infty}^{+\infty} \epsilon(t) e^{-j\omega(t)}\, dt$$

and the subscripts d and p indicate the detector and the absorber positions respectively and $\epsilon(t)$ is the absorber amplitude of motion. The term γ is an absorber factor characterizing the strength of the absorber. In the development of equation (3.6), second and higher order terms in the Taylor's series are dropped, therefore equation (3.6) is valid only for a weak absorber. Once $\Psi(r,\vec{\omega})$ is determined by solving equation (3.4), the detector response, dR, can be calculated using equation (3.6).

In this work $\Psi(\vec{r},\omega)$ was determined by solving equation (3.4) using the polynomial nodal model. The polynomial nodal model was also used in determining the static flux, ϕ. The adjoint function, Ψ, and the static flux, ϕ, were obtained in the form of a polynomial as a function of position as shown in Chapter IV. Using these two functions, the detector response, dR, was calculated from equation (3.6).

In two-dimensional rectangular coordinates, equation (3.6) can be expressed as follows (13):

$$dR(x_d,x_p,y_d,y_p,\omega) =$$

$$\left[\psi(x_d,x,y_d,y,\omega)\,\frac{\partial\phi(x,y)}{\partial x} + \phi(x,y)\,\frac{\partial\psi(x_d,x,y_d,y,\omega)}{\partial x}\right]_{x=x_p,y=y_p} \delta x(\omega)$$

$$+\left[\psi(x_d,x,y_d,y,\omega)\,\frac{\partial\phi(x,y)}{\partial y} + \phi(x,y)\,\frac{\partial\psi(x_d,x,y_d,y,\omega)}{\partial x}\right]_{x=x_p,y=y_p} \delta y(\omega) \quad 3.7$$

where x_p and y_p are the coordinates of the perturbation point and $\delta x(\omega)$ and $\delta y(\omega)$ are the Fourier Transforms of the x and y components of the vibrator motion. The value of γ is constant and is assumed to be unity for normalization purpose. Equation (3.7) was used in the computer code GPLOT to calculate the detector response.

B. One-Energy Group Diffusion Theory Model

The steady state one energy group diffusion equation is

$$D\nabla^2\phi - \Sigma_a\phi + \frac{\nu\Sigma_f}{K}\phi = 0. \qquad 3.8$$

where

- D - Diffusion coefficient
- Σ_a - Absorption cross section
- ν - Number of neutrons produced per fission
- Σ_f - Fission cross section
- ϕ - Flux

Equation (3.8) was used in a one-energy group computer code to calculate the eigenvalue, K, and the static flux, ϕ.

The general one-energy group and one delayed group equations in the time domain, are given by

$$D\nabla^2\phi - \Sigma_a\phi + (1-\beta)\nu\Sigma_f\phi + \lambda C = \frac{1}{v}\frac{\partial\phi}{\partial t} \qquad 3.9$$

$$\beta\nu\Sigma_f\phi - \lambda C = \frac{\partial C}{\partial t} \qquad 3.10$$

where

v = Average neutron velocity

λ = Decay constant

C = Precursor concentration

β = Delayed neutron fraction

Equation (3.9) and (3.10) are the one-energy group approximations of equation (3.1).

The changes in Σ_a, ϕ and C assuming the absorption cross section is the only parameter affected by the vibration, is given by

$$\Sigma_a = \Sigma_a^o + \delta\Sigma_a \qquad 3.11a$$

$$\phi = \phi^o + \delta\phi \qquad 3.11b$$

$$C = C^o + \delta C \qquad 3.11c$$

where the superscript o indicates steady state values.

Substituting equations (3.11a) to (3.11c) into equations (3.9) and (3.10) and canceling the steady state terms yields

$$D\nabla^2\delta\phi - \Sigma_a^o\delta\phi - \phi^o\delta\Sigma_a + (1-\beta)\nu\Sigma_f\delta\phi + \lambda\delta C = \frac{1}{v}\frac{\partial\delta\phi}{\partial t} \qquad 3.12$$

$$\beta\nu\Sigma_f\delta\phi - \lambda\delta C = \frac{\partial\delta C}{\partial t} \qquad 3.13$$

The term $\delta\phi\delta\Sigma_a$ will be very small compared to the rest of the terms and is assumed to be negligible.

Application of the Fourier Transform to equations (3.12) and (3.13) yield, upon elimination of the precursor term,

$$D\nabla^2\Delta\phi - \Sigma_a^o\Delta\phi + \nu\Sigma_f(1 - \frac{j\omega\beta}{j\omega+\lambda})\Delta\phi - j\frac{\omega}{v}\Delta\phi = \phi^o\delta\Sigma_a \qquad 3.14$$

where $\Delta\phi$ is the Fourier Transform of $\delta\phi$. Equation (3.14) is the one-energy group approximation of equation (3.2). For the one-group case, the detector adjoint function, Ψ, will be the same as $\Delta\phi$. Therefore, equation (3.14) in terms of the detector adjoint function, Ψ, will be

$$D\nabla^2\Psi - \Sigma_a^o\Psi + \nu\Sigma_f(1 - \frac{j\omega\beta}{j\omega+\lambda})\Psi - j\frac{\omega}{v}\Psi = \phi^o\delta\Sigma_a \qquad 3.15$$

The detector adjoint function, Ψ, is complex and mathematically can be expressed in terms of a real and an imaginary component as follows:

$$\Psi = \psi + j\chi \qquad 3.16$$

where

ψ = Real part of Ψ

χ = Imaginary part of Ψ

Substituting the real and imaginary parts of Ψ in equation (3.15) and collecting the real and imaginary terms will result in the following set of equations:

$$\nabla^2\psi + \alpha\psi + \beta\chi = \delta(x-x_d)\delta(y-y_d) \qquad 3.17$$

$$\nabla^2\chi - \beta\psi + \alpha\chi = 0 \qquad 3.18$$

where

$$\alpha = \frac{1}{D}[-\Sigma_a + \nu\Sigma_f(1 - \frac{\beta\omega^2}{\omega^2 + \lambda^2})]$$

$$\beta = \frac{1}{D}[\nu\Sigma_f(\frac{\beta\lambda\omega}{\omega^2 + \lambda^2}) + \frac{\omega}{v}]$$

The coordinates (x_d, y_d) indicate the detector location.

Equation (3.17) is a non-homogenous equation and can be solved by applying the Green's function technique, subject to the usual free surface boundary conditions and the continuity of the adjoint currents at region interfaces plus the usual Green's function boundary conditions at the detector, namely

$$\psi(x,\omega)\Big|_{x_{d+0}} = \psi(x,\omega)\Big|_{x_{d-0}} \qquad 3.19a$$

$$\chi(x,\omega)\Big|_{x_{d+0}} = \chi(x,\omega)\Big|_{x_{d-0}} \qquad 3.19b$$

$$\frac{\partial\chi(x,\omega)}{\partial x}\Big|_{x_{d+0}} - \frac{\partial\chi(x,\omega)}{\partial x}\Big|_{x_{d-0}} = 0 \qquad 3.19c$$

$$D\frac{\partial\psi(x,\omega)}{\partial x}\Big|_{x_{d+0}} - D\frac{\partial\psi(x,\omega)}{\partial x}\Big|_{x_{d-0}} = -1 \qquad 3.19d$$

Equations (3.17) and (3.18) were used to calculate the detector adjoint function, Ψ, as if these are two-energy group equations. The detector response, dR, was calculated using equation (3.7). The phase angle, τ, was calculated as follows:

$$\tau = \tan^{-1}(\frac{\chi}{\psi}) \qquad 3.20$$

C. Development of Analytical Solution

Comparing equation (3.12) with equation (1) of Pazsit and Analytis (13) one has

$$B(\omega)^2 = \frac{1}{D}\left[\nu\Sigma_f\left(1 - \frac{j\omega\beta}{j\omega+\lambda} \right) - \Sigma_a - j\frac{\omega}{v}\right] \qquad 3.21$$

Therefore, equation (3.15) in x and y coordinates is given by

$$\nabla^2\Psi(x,y,x_d,y_d,\omega) + B(\omega)^2\Psi(x,y,x_d,y_d,\omega) = \delta(x-x_d)\delta(y-y_d) \qquad 3.22$$

where x_d and y_d indicate detector position.

The detector adjoint function is assumed to vanish at the boundary, i.e.,

$$\Psi(x=0,y=b) = \Psi(x=0,y=0) = 0 \qquad 3.23a$$

$$\Psi(x=a,y=0) = \Psi(x=a,y=b) = 0 \qquad 3.23b$$

where a and b are the dimensions of the reactor.

Using the classical Green's function solution, the detector adjoint function is expanded in a double summation sine series as follows (28):

$$\Psi(x,y,x_d,y_d,\omega) = \sum_{m,n=1}^{\infty} H_{mn} \sin(B_n x) \sin(A_m y) \qquad 3.24$$

where

$$B_n = \frac{n\pi}{a}$$

$$A_m = \frac{m\pi}{b}$$

Equation (3.22) was solved for H_{mn} using the boundary conditions given by equations (3.19) and (3.23) and using the properties of the

δ-function. Therefore, the detector adjoint function can be written in a double sine series expansion as (13)

$$\Psi(x,y,x_d,y_d,\omega) = -\left(\frac{4}{ab}\right)\sum_{m,n=1}^{\infty} \frac{\sin(B_n x)\,\sin(B_n x_d)\,\sin(A_m y)\,\sin(A_m y_d)}{B_n^2 + A_m^2 - B(\omega)^2} \qquad 3.25$$

Equation (3.25) is an analytical solution of the detector adjoint function for the one-energy group, two-dimensional homogenous reactor.

D. Two-Energy Group Diffusion Theory Model

The steady state two-energy group diffusion equations are

$$D_1\nabla^2\phi_1 - \Sigma_1\phi_1 - \Sigma_{12}\phi_1 + \frac{1}{K}(\nu\Sigma_{f1}\phi_1 + \nu\Sigma_{f2}\phi_2) = 0 \qquad 3.26$$

$$D_2\nabla^2\phi_2 - \Sigma_2\phi_2 + \Sigma_{12}\phi_1 = 0 \qquad 3.27$$

where subscripts 1 and 2 indicate the fast and thermal energy groups respectively. Subscript 12 indicates neutron scattering from energy group 1 to 2. Equations (3.25) and (3.26) were used in a two-energy group computer code to determine the eigenvalue, K, and the static flux, ϕ.

The two-energy group neutron diffusion equations and the one-group delayed neutron precursor equation, which describe the small stochastic fluctuations of the neutron flux induced by small stochastic

fluctuations of the thermal absorption cross section parameters, are given, in the time domain by

$$D_1\nabla^2\phi_1 - \Sigma_1\phi_1 - \Sigma_{12}\phi_1 + (1-\beta)(\nu\Sigma_{f1}\phi_1 + \nu\Sigma_{f2}\phi_2) + \lambda C - \frac{1}{v_1}\frac{\partial\phi_1}{\partial t} \qquad 3.28$$

$$D_2\nabla^2\phi_2 - \Sigma_2\phi_2 + \Sigma_{12}\phi_1 = \frac{1}{v_2}\frac{\partial\phi_2}{\partial t} \qquad 3.29$$

$$\beta(\nu\Sigma_{f1}\phi_1 + \nu\Sigma_{f2}\phi_2) - \lambda C = \frac{\partial C}{\partial t} \qquad 3.30$$

Equations (3.28), (3.29) and (3.30) are the two-energy group approximation of equation (3.1). The change in parameters, assuming the thermal group absorption cross section is the only cross section affected by the vibration, is given by

$$\Sigma_2 = \Sigma_2^o + \delta\Sigma_2 \qquad 3.31a$$

$$\phi_1 = \phi_1^o + \delta\phi_1 \qquad 3.31b$$

$$\phi_2 = \phi_2^o + \delta\phi_2 \qquad 3.31c$$

$$C = C^o + \delta C \qquad 3.31d$$

where superscript o indicates the steady state parameters.

Substituting equations (3.31a) to (3.31d) in equations (3.28) and (3.29), cancelling steady state terms, applying the Fourier Transform

and eliminating the precursor term will result in the following set of equations:

$$D_1\nabla^2\Delta\phi_1 - \Sigma_1\Delta\phi_1 - \Sigma_{12}\Delta\phi_1 + (1 - \frac{j\beta\omega}{\lambda+j\omega})(\nu\Sigma_{f1}\Delta\phi_1 + \nu\Sigma_{f2}\Delta\phi_2) - \frac{j\omega}{v_1}\Delta\phi_1 = 0. \quad 3.32$$

$$D_2\nabla^2\Delta\phi_2 - \Sigma_2^o\Delta\phi_2 + \Sigma_{12}^o\Delta\phi_1 - \frac{j\omega}{v_2}\Delta\phi_2 = \phi_2^o\delta\Sigma_2 \quad 3.33$$

where $\Delta\phi$ represents the fourier Transform of $\delta\phi$. The term $\delta\phi\delta\Sigma_2$ is very small compared to other terms in the equation and is assumed to be negligible. Equations (3.32) and (3.33) are the two-energy group approximation of equation (3.2).

Equations (3.32) and (3.33) can be written in matrix form as follows:

$$\begin{bmatrix} D_1\nabla^2 - \Sigma_1^o - \Sigma_{12}^o + \nu\Sigma_{f1}(1 - \frac{j\beta\omega}{j\omega+\lambda}) - j\frac{\omega}{v_1} & \nu\Sigma_{f2}(1 - \frac{j\beta\omega}{j\omega+\lambda}) \\ \Sigma_{12} & D_2\nabla^2 - \Sigma_2 - j\frac{\omega}{v_2} \end{bmatrix} \begin{bmatrix} \Delta\phi_1 \\ \Delta\phi_2 \end{bmatrix} = - \begin{bmatrix} 0 \\ \phi_2^o\delta\Sigma_2 \end{bmatrix} \quad 3.34$$

Therefore, the adjoint of the equation (3.34) will be as follows:

$$\begin{bmatrix} D_1\nabla^2 - \Sigma_1^o - \Sigma_{12}^o + \nu\Sigma_{f1}\left(1 - \frac{j\beta\omega}{j\omega+\lambda}\right) - j\frac{\omega}{v_1} & \Sigma_{12} \\ \nu\Sigma_{f2}\left(1 - \frac{j\beta\omega}{j\omega+\lambda}\right) & D_2\nabla^2 - \Sigma_2 - j\frac{\omega}{v_2} \end{bmatrix} \begin{bmatrix} \Psi_1 \\ \Psi_2 \end{bmatrix} = \begin{bmatrix} 0 \\ \phi_2^o \delta\Sigma_2 \end{bmatrix} \qquad 3.35$$

where Ψ_1 and Ψ_2 are the fast and thermal detector adjoint functions respectively and are complex in nature.

Substituting the real, ψ, and imaginary, χ, parts for Ψ_1 and Ψ_2 and collecting the real and imaginary terms will result in a set of four equations.

$$\nabla^2\psi_1 + \alpha_1\psi_1 + \alpha_2\psi_2 + \alpha_3\chi_1 + \alpha_4\chi_2 = 0 \qquad 3.36$$

$$\nabla^2\psi_2 + \beta_1\psi_1 + \beta_2\psi_2 + \beta_3\chi_1 + \beta_4\chi_2 = \delta(x-x_0)\delta(y-y_0) \qquad 3.37$$

$$\nabla^2\chi_1 - \alpha_3\psi_1 + \alpha_4\psi_2 + \alpha_1\chi_1 + \alpha_2\chi_2 = 0 \qquad 3.38$$

$$\nabla^2\chi_2 - \beta_3\psi_1 - \beta_4\psi_2 + \beta_1\chi_1 + \beta_2\chi_2 = 0 \qquad 3.39$$

where

$$\alpha_1 = \frac{1}{D_1}\left[-\Sigma_1 - \Sigma_{12} + \nu\Sigma_{f1}\left(1 - \frac{\beta\omega^2}{\omega^2 + \lambda^2}\right)\right]$$

$$\alpha_2 = \frac{\Sigma_{12}}{D_1}$$

$$\alpha_3 = \frac{1}{D_1}\left[\nu\Sigma_{f1}\left(\frac{\beta\lambda\omega}{\omega^2 + \lambda^2}\right) + \frac{\omega}{v_1}\right]$$

$$\alpha_4 = 0$$

$$\beta_1 = \frac{1}{D_2}\Sigma_{f2}\left(1 - \frac{\beta\omega^2}{\omega^2 + \lambda^2}\right)$$

$$\beta_2 = -\frac{\Sigma_2}{D_2}$$

$$\beta_3 = \frac{1}{D_2}\nu\Sigma_{f2}\left(\frac{\beta\lambda\omega}{\omega^2 + \lambda^2}\right)$$

$$\beta_4 = \frac{\omega}{D_2 v_2}$$

Equation (3.37) is a non-homogenous equation and can be solved by applying the Green's function technique, subject to the usual free surface boundary conditions and the continuity of the adjoint currents at region interfaces plus the usual Green's function boundary conditions at the detector, namely

$$\Psi_1(x,\omega)\Big|_{x_{d+0}} = \Psi_1(x,\omega)\Big|_{x_{d-0}} \qquad 3.40a$$

$$\Psi_2(x,\omega)\Big|_{x_{d+0}} = \Psi_2(x,\omega)\Big|_{x_{d-0}} \qquad 3.40b$$

$$\left.\frac{\partial \Psi_1(x,\omega)}{\partial x}\right|_{x_{d+0}} - \left.\frac{\partial \Psi_1(x,\omega)}{\partial x}\right|_{x_{d-0}} = 0 \qquad 3.40c$$

$$\left.\frac{\partial \chi_2(x,\omega)}{\partial x}\right|_{x_{d+0}} - \left.\frac{\partial \chi_2(x,\omega)}{\partial x}\right|_{x_{d-0}} = 0 \qquad 3.40d$$

$$D_2\left.\frac{\partial \psi_2(x,\omega)}{\partial x}\right|_{x_{d+0}} - D_2\left.\frac{\partial \psi_2(x,\omega)}{\partial x}\right|_{x_{d-0}} = -1 \qquad 3.40e$$

Equations (3.36) to (3.38) were used to calculate the detector adjoint functions treating them as the standard four-energy group equations. The detector response, dR, is calculated using equation (3.7).

IV. COMPUTER NODAL MODEL DEVELOPMENT

A. Rohach (7) developed the polynomial nodal model technique to solve the one-dimensional multi-energy neutron group diffusion equations. M. Feiz (9) applied the technique to determine the power distribution in an operating reactor. In this technique, the neutron flux is expanded in polynomials. A similar one-dimensional two-energy neutron group computer code was developed using the nodal model technique to solve for the Green's function using the source conditions as described in the previous chapter. This computer code is called ONED2G. A one-dimensional Green's function for the Iowa State University UTR-10 reactor was obtained using the ONED2G computer code. The results obtained with this computer code were compared against the analytical solution developed by Al-Ammar (11) and are described in the following chapter.

In the remainder of this chapter, the efforts will be concentrated on the development of the two-dimensional polynomial nodal model to solve the diffusion equations or Green's function for one or two energy neutron groups.

Rohach (8) used fourth order Legendre Polynomials to approximate the flux compared to a straight power series used for this research. In the polynomial nodal model the cross sections and diffusion coefficients of each node are assigned independently. Two adjacent nodes can have different material properties but in any given node

the material properties are taken to be homogeneous. Each node is treated independently and is connected to adjacent nodes by the interface conditions. The flux in each node, for a given energy group, is expressed in the form of a fourth order polynominal and is approximated as follows:

$$\phi_{ij} = \sum_{m=0}^{4} \sum_{n=0}^{4-m} a_{mn} x^m y^n \qquad 4.1$$

where a_{mn} are unknown coefficients of the polynomial and depend upon the material properties of the node(i,j). There are fifteen unknown coefficients in equation (4.1) but since only fourteen boundary conditions were developed, a coefficient a_{22} in equation (4.1) is discarded. Therefore, fourteen conditions are developed for each energy group flux to evaluate these fourteen unknown coefficients.

A. Minimization of the Error in the Flux Approximation

Since the polynomial solutions are only approximations, one- and two-energy group diffusion equations (3.8), (3.26) and (3.27) used in an eigenvalue calculation and equations (3.17), (3.18) and equations (3.36) to (3.39) used to solve for the detector adjoint function are not equal to zero. The function g(x,y) called the residual of the diffusion approximation can be expressed as follows.

$$\nabla^2 \phi_1 + \alpha_1 \phi_1 + \alpha_2 \phi_2 = g(x,y) \qquad 4.2$$

The constant α depends upon the material properties of the node and is calculated as shown in Chapter III. Subscripts 1 and 2 refer to the fast and thermal neutron energy groups respectively. Equation (4.2) in a multi-energy group formulation can be written as follow:

$$\nabla^2\phi_1 + \sum_{g=0}^{G} \alpha_g \phi_g = g(x,y) \qquad 4.3$$

where G is the number of energy groups.

The fluxes ϕ_g in the second term on the left side of equation (4.3) are assumed to be known from a previous iteration in the numerical solution and are redefined as $\tilde{\phi}_g$. Therefore, the derivative of $\tilde{\phi}_g$ with respect to any variable will be taken as zero. Redefining the Laplacian operator in equation (4.3) as

$$\nabla^2\phi_1 = \left(\frac{\partial^2}{\partial x^2} + \frac{\partial^2}{\partial y^2} \right)\phi_1 \qquad 4.4$$

and substituting equation 4.1 into (4.4), equation (4.4) yields

$$\begin{aligned}\nabla^2\phi_1 = {} & 2a_{20} + 6a_{30}x + 12a_{40}x^2 + 2a_{21}y + 6a_{31}xy \\ & + 2a_{02} + 6a_{03}y + 12a_{04}y^2 + 2a_{12}x + 6a_{13}xy \end{aligned} \qquad 4.5$$

A least square minimization of the integrated residual over the volume of node(i,j), with respect to the polynomial coefficient; a_{mn}, will be taken as zero to minimize the residual term.

$$\frac{\partial}{\partial a_{mn}} \int_{vol} g^2(x,y) = 0 \qquad 4.6$$

By the use of Leibnitz's rule, equation (4.6) will be

$$\frac{\partial}{\partial a_{mn}} \int_{vol} g^2(x,y)dv = 2\int_{vol} g(x,y) \frac{\partial g(x,y)}{\partial a_{mn}} dv = 0 \qquad 4.7$$

and

$$\int_{-\eta}^{\eta} \int_{-\nu}^{\nu} g(x,y) \frac{\partial g(x,y)}{\partial a_{mn}} dxdy = 0 \qquad 4.8$$

B. Development of Conditions for Coefficients

Each boundary surface of the node is divided into two equal segments. The average value of the flux from the property of continuity of the flux at the interface of the surface will be applied.

Therefore, from Figure 4.1

$$F^{RT}_{i,j} = F^{LT}_{i+1,j} \qquad 4.9a$$

$$F^{RB}_{i,j} = F^{LB}_{i+1,j} \qquad 4.9b$$

$$F^{TL}_{i,j} = F^{BL}_{i,j+1} \qquad 4.9c$$

$$F^{TR}_{i,j} = F^{BR}_{i,j+1} \qquad 4.9d$$

$$F^{LT}_{i,j} = F^{RT}_{i-1,j} \qquad 4.9e$$

$$F^{LB}_{i,j} = F^{RB}_{i-1,j} \qquad 4.9f$$

$$F^{BL}_{i,j} = F^{TL}_{i,j-1} \qquad 4.9g$$

$$F^{BR}_{i,j} = F^{TR}_{i,j-1} \qquad 4.9h$$

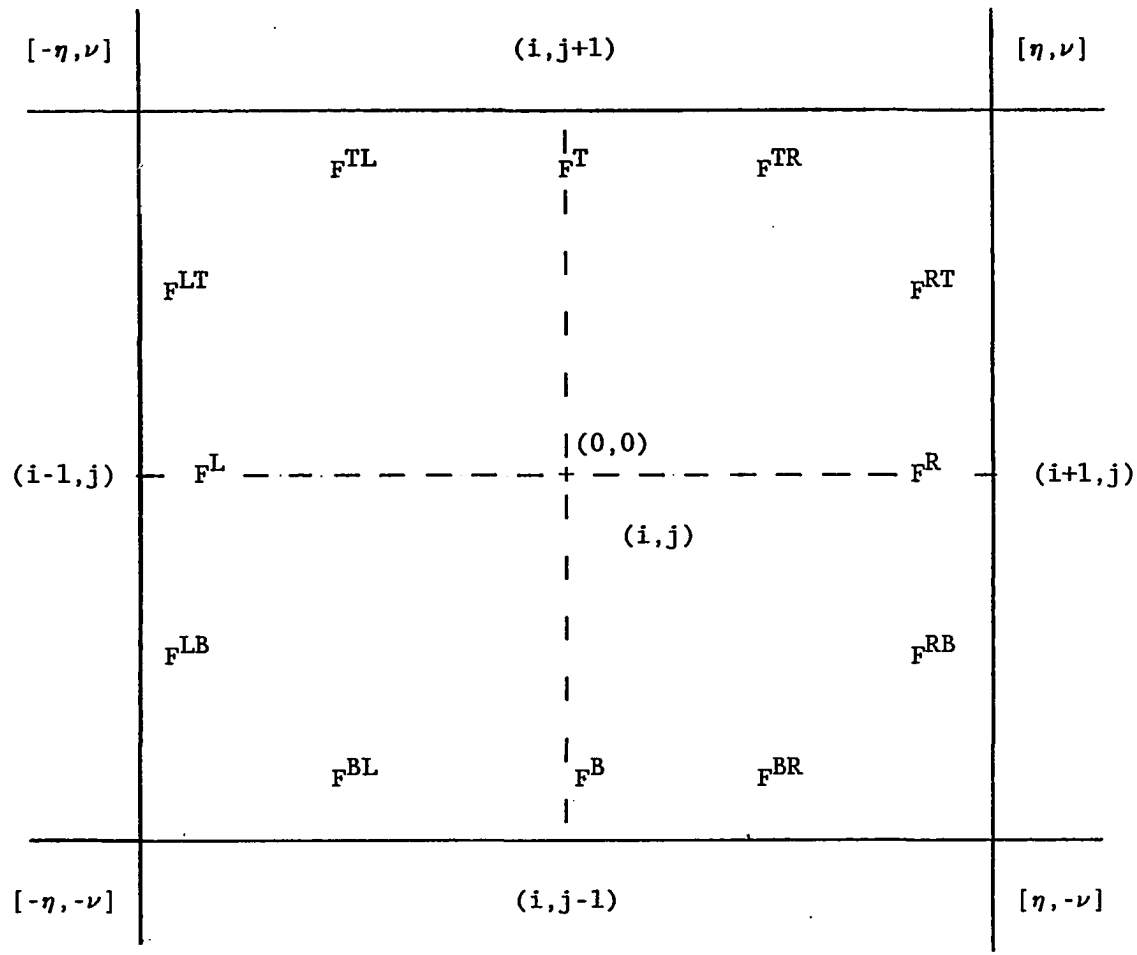

Figure 4.1. Nodal geometry for average boundary fluxes

Using the polynomial expressions, the average flux F_{ij}^{RT} is

$$F_{ij}^{RT} = \left. \frac{\int_0^\nu \phi_{ij}(x,y)\, dy}{\int_0^\nu dy} \right|_{x=\eta} \tag{4.10a}$$

$$= \left. \frac{\int_0^\nu \sum_{m=0}^{4} \sum_{n=0}^{4-m} a_{ij} x^m y^n \, dy}{\int_0^\nu dy} \right|_{x=\eta} \tag{4.10b}$$

$$F_{ij}^{RT} = \frac{1}{\nu}\int_0^\nu [a_0 + a_{10}x + a_{20}x^2 + a_{30}x^3 + a_{40}x^4 + a_{11}xy + a_{01}y + a_{02}y^2 + a_{03}y^3 + a_{04}y^4 + a_{12}xy^2 + a_{21}x^2y + a_{13}xy^3 + a_{31}x^3y]dy \tag{4.11a}$$

$$= a_0 + a_{10}\eta + a_{20}\eta^2 + a_{30}\eta^3 + a_{40}\eta^4 + \frac{1}{2}a_{11}\eta\nu + \frac{1}{2}a_{01}\nu + \frac{1}{3}a_{02}\nu^2 + \frac{1}{5}a_{04}\nu^4 + \frac{1}{2}a_{21}\eta^2\nu + \frac{1}{3}a_{12}\eta\nu^2 + \frac{1}{2}a_{31}\eta^3\nu + \frac{1}{4}a_{13}\eta\nu^3 \tag{4.11b}$$

Similarly, the values of the remaining average fluxes at the interface of the node can be evaluated.

From equations (4.3) and (4.5)

$$\frac{\partial g(x,y)}{\partial a_{20}} = 2 \tag{4.12}$$

$$\frac{\partial g(x,y)}{\partial a_{12}} = 2x \tag{4.13}$$

$$\frac{\partial g(x,y)}{\partial a_{21}} = 2y \qquad 4.14$$

$$\frac{\partial g(x,y)}{\partial a_{31}} = 6xy \qquad 4.15$$

$$\frac{\partial g(x,y)}{\partial a_{40}} = 12x^2 \qquad 4.16$$

$$\frac{\partial g(x,y)}{\partial a_{04}} = 12y^2 \qquad 4.17$$

From the above six equations (4.12) to (4.17) and the equations (4.9a) to (4.9h) for the eight interface fluxes; fourteen unknowns are evaluated.

C. Development of Coefficients

An example for evaluating the coefficient a_{20} will be given.

Upon substituting the value of $g(x,y)$ and $\frac{\partial g(x,y)}{\partial a_{20}}$ in equation (4.9) and integrating over the node volume the expression for the coefficient a_{20} can be written as follow:

$$a_{20} = -\frac{1}{2}(4\eta^2 a_{40} + 4\nu^2 a_{40}) - \lambda_1 - a_{02} \qquad 4.18$$

where

$$\lambda_1 = \sum_{g=0}^{G} \alpha_g \left(\tilde{a}_0^g + \frac{1}{3}\tilde{a}_{20}^g \eta^2 + \frac{1}{5}\tilde{a}_{40}^g \eta^4 + \frac{1}{3}\tilde{a}_{02}^g \nu^2 + \frac{1}{5}\tilde{a}_{04}^g \nu^4\right)$$

The coefficients $\tilde{a}^g$ represent the neutron energy group g and are assumed known from a previous iteration in the numerical solution. The

parameter α_g are derived from the material properties of the node as shown in Chapter III. Therefore, the term λ_1 is also assumed known from the previous iteration. By adding the equations (4.9a), (4.9b), (4.9e) and (4.9f) and then subtracting the equations (4.9c), (4.9d), (4.9g) and (4.9h), the coefficient a_{02} can be written as

$$a_{02} = \frac{3}{4}\nu^2\left(\frac{8}{5}a_{40}\eta^4 - \frac{8}{5}a_{04}\nu^4 - \gamma_1\right) + a_{20}\frac{\eta^2}{\nu^2} \qquad 4.19$$

where

$$\gamma_1 = F^R + F^L - F^T - F^B$$

$$F^R = (F^{RT} + F^{RB})/2 = \int_{-\nu}^{\nu}\phi(x,y)dy \Big/ \int_{-\nu}^{\nu}dy$$

$$F^T = (F^{TL} + F^{TR})/2 = \int_{-\eta}^{\eta}\phi(x,y)dx \Big/ \int_{-\eta}^{\eta}dx$$

$$F^L = (F^{LT} + F^{LB})/2 = \int_{-\nu}^{\nu}\phi(x,y)dy \Big/ \int_{-\nu}^{\nu}dy$$

$$F^B = (F^{BL} + F^{BR})/2 = \int_{-\eta}^{\eta}\phi(x,y)dx \Big/ \int_{-\eta}^{\eta}dx$$

F^R, F^T, F^L, and F^B are assumed known from a previous iteration. Upon substituting the value of a_{02} in equation (4.18) and rewriting the equation for a_{20} one has

$$a_{20} = \frac{3}{4(\eta^2 + \nu^2)}\left(\gamma_1 - \frac{8}{15}a_{40}(3\eta^4 + 5\eta^2\nu^2) - \frac{16}{15}a_{04}\nu^4 - \frac{2}{3}\nu^2\lambda_1\right) \qquad 4.20$$

Similarly the remaining 13 coefficients were evaluated and are listed as follows:

$$a_{02} = \frac{3}{4(\eta^2 + \nu^2)}(\gamma_1 - \frac{8}{15}a_{04}(3\nu^4 + 5\eta^2\nu^2) - \frac{16}{15}a_{40}\eta^4 - \frac{2}{3}\eta^2\lambda_1) \quad 4.21$$

$$a_{03} = -\frac{1}{3}(\frac{3\gamma_2 + 2\nu\eta^2\lambda_{12}}{\nu^3 + 4\nu\eta^2}) \quad 4.22$$

$$a_{30} = -\frac{1}{3}(\frac{3\gamma_2 + 2\eta\nu^2\lambda_{21}}{\eta^3 + 4\eta\nu^2}) \quad 4.23$$

$$a_{12} = \frac{1}{2}(\frac{6\gamma_2 + \eta^3\lambda_{21}}{\eta^3 + 4\eta\nu^2}) \quad 4.24$$

$$a_{21} = \frac{1}{2}(\frac{6\gamma_2 + \nu^3\lambda_{12}}{\nu^3 + 4\nu\eta^2}) \quad 4.25$$

$$a_{10} = \frac{1}{6\eta}(3(F^R - F^L) - 2(a_{12}\eta\nu^2 - 6a_{30}\eta^3)) \quad 4.26$$

$$a_{01} = \frac{1}{6\nu}(3(F^T - F^B) - 2(a_{21}\nu\eta^2 - 6a_{03}\nu^3)) \quad 4.27$$

$$a_{31} = (\frac{6\gamma_3 - \eta\nu^3\lambda_3}{6(\eta\nu^3 + \nu\eta^3)}) \quad 4.28$$

$$a_{13} = -(\frac{6\gamma_3 + \nu\eta^3\lambda_3}{6(\eta\nu^3 + \nu\eta^3)}) \quad 4.29$$

$$a_{11} = \frac{1}{4\eta\nu}(\gamma_4 - 3a_{31}\eta^3\nu - 3a_{13}\eta\nu^3) \quad 4.30$$

$$a_{40} = -\frac{1}{12}\sum_{g=0}^{G}\alpha_g(\tilde{a}^g_{20} + \frac{6}{7}\tilde{a}^g_{40}\eta^2) \qquad 4.31$$

$$a_{04} = -\frac{1}{12}\sum_{g=0}^{G}\alpha_g(\tilde{a}^g_{02} + \frac{6}{7}\tilde{a}^g_{04}\nu^2) \qquad 4.32$$

$$a_0 = \frac{1}{4}(F^R + F^T + F^L + F^B - \frac{8}{3}a_{20}\eta^2 - \frac{8}{3}a_{02}\nu^2 - \frac{12}{5}a_{40}\eta^4 - \frac{12}{5}a_{04}\nu^4) \qquad 4.33$$

where

$$\gamma_2 = F^L - F^R - F^{TR} - F^{TL} + F^{BR} - F^{BL}$$

$$\gamma_3 = F^{RT} - F^{TL} + F^{LB} + F^{BR} - (F^{RB} + F^{TR} + F^{LT} + F^{BL})$$

$$\gamma_4 = F^{RT} + F^{TR} + F^{LB} + F^{BL} - (F^{RB} + F^{TL} + F^{LT} + F^{BR})$$

$$\lambda_{12} = \sum_{g=0}^{G}\alpha_g(\tilde{a}^g_{01} + \frac{3}{5}\tilde{a}^g_{03}\nu^2 + \frac{1}{3}\tilde{a}^g_{21}\eta^2)$$

$$\lambda_{21} = \sum_{g=0}^{G}\alpha_g(\tilde{a}^g_{01} + \frac{3}{5}\tilde{a}^g_{03}\eta^2 + \frac{1}{3}\tilde{a}^g_{21}\nu^2)$$

$$\lambda_3 = \sum_{g=0}^{G}\alpha_g(\tilde{a}^g_{11} + \frac{3}{5}\tilde{a}^g_{31}\eta^2 + \frac{1}{3}\tilde{a}^g_{13}\nu^2)$$

Similarly, the expressions for the coefficients of the polynomials for the second, third, and fourth group were derived.

D. Interface Condition

From the diffusion theory condition of the continuity of flux,

$$\phi_{i,j} = \phi_{i+1,j} \qquad 4.34$$

must be applied at any interface as shown in Figure 4.2. The fluxes $\phi_{i,j}$ and $\phi_{i+1,j}$ are the average fluxes and are evaluated using the polynomial constants of node (i,j) and (i+1,j) respectively.

The interface current condition between the two nodes as shown in Figure 4.2 is based on the average fluxes. The net current, J, at any interface can be defined as

$$J = -D\frac{\partial\phi(x,y)}{\partial x} \qquad 4.35$$

where

D = Diffusion coefficient

The average value of current is determined by first determining the average flux and than differentiating it with respect to the direction.

i.e.

$$-D\frac{\partial\bar{\phi}}{\partial x} = -D\left[\frac{\partial(\int\phi(x,y)dy/\int dy)}{\partial x}\right] \qquad 4.36$$

Using the property of the continuity of current at the interface, the average flux for the new iteration will be evaluated. Therefore,

$$J_{i,j} = J_{i+1,j} \qquad 4.37$$

From Figure 4.2

$$-D_{i,j}\frac{\partial\bar{\phi}_{i,j}}{\partial x}\bigg|_{x=\eta_i} = -D_{i+1,j}\frac{\partial\bar{\phi}_{i+1,j}}{\partial x}\bigg|_{x=\eta_{i+1}} \qquad 4.38$$

where $D_{i,j}$ and $D_{i+1,j}$ are the diffusion coefficients of node (i,j) and node (i+1,j) respectively. The fluxes $\bar{\phi}_{i,j}$ and $\bar{\phi}_{i+1,j}$ are the average

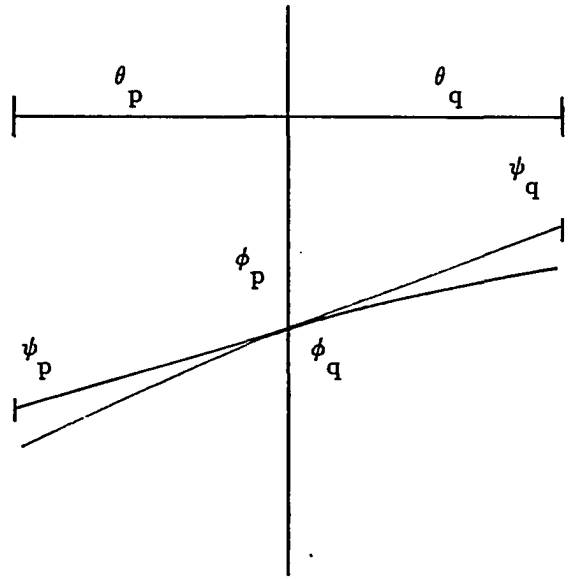

Figure 4.2. Assumed flux profile at the interface

fluxes calculated using the constants of polynomial of node (i,j) and node (i+1,j) respectively.

Using the finite difference approximation, from equations (4.35) and (4.37) one has

$$D_{i,j}\left(\frac{\overline{\phi}_{i,j} - \overline{\psi}_{i,j}}{\theta_{i,j}}\right) = D_{i+1,j}\left(\frac{\overline{\psi}_{i+1,j} - \overline{\phi}_{i+1,j}}{\theta_{i+1,j}}\right) \qquad 4.39$$

where

$\overline{\phi}_{i,j}$ = Average flux evaluated at node interface using the properties of node (i,j)

$\overline{\psi}_{i,j}$ = Average flux evaluated at distance $\theta_{i,j}$ away from node interface using the properties of node (i,j)

$\overline{\phi}_{i+1,j}$ = Average flux evaluated at node interface using the properties of node (i+1,j)

$\overline{\psi}_{i+1,j}$ = Average flux evaluated at distance $\theta_{i+1,j}$ away from node interface using the properties node (i+1,j)

θ = Distance parameters

From equations (4.34) and (4.39), $\overline{\phi}_{i,j}$ at the node interface can be evaluated to be

$$\overline{\phi}_{i,j} = \overline{\phi}_{i+1,j}$$

$$= \frac{D_{i+1,j}\theta_{i,j}\overline{\psi}_{i+1,j} + D_{i,j}\theta_{i+1,j}\overline{\psi}_{i,j}}{D_{i,j}\theta_{i+1,j} + D_{i+1,j}\theta_{i,j}} \qquad 4.40$$

E. Boundary Conditions

A concept of "extrapolation distance" is used to evaluate the flux at the boundary (14,29). The reactor extrapolation distance is a mathematical condition that implies the flux vanishes at the extrapolated distance beyond the edge of the free surfaces and can be expressed as follows:

$$D \frac{d\phi}{dx} = - \tau\phi \qquad 4.41$$

where

D/τ = extrapolation distance; cm.

The value of τ can be evaluated either using the albedo boundary condition concept (14,29) or from the transport theory (30). In most cases the extrapolation distance is small compared to the size of the reactor so the flux is assumed to vanish at the core boundary.

F. Source Interface Conditions

In one-dimensional geometry a plane source is positioned at the interface of two adjacent nodes. The source position is identified by the node (i) as shown in Figure 4.3. In the case of two-dimensional geometry a crucifix "+" shape source which represents intersecting source planes, is simulated as shown in Figure 4.4. Each wing of the source extends across one half node. The source position is identified

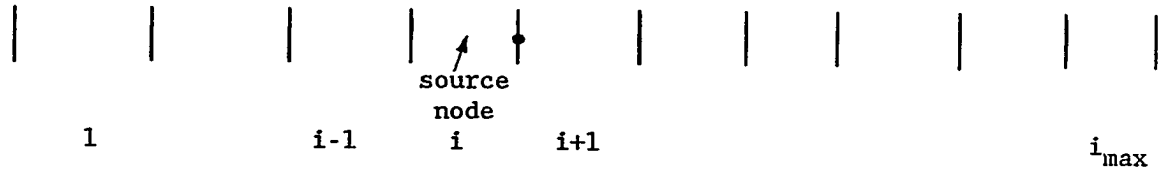

Figure 4.3. Source geometry for one-dimensional code

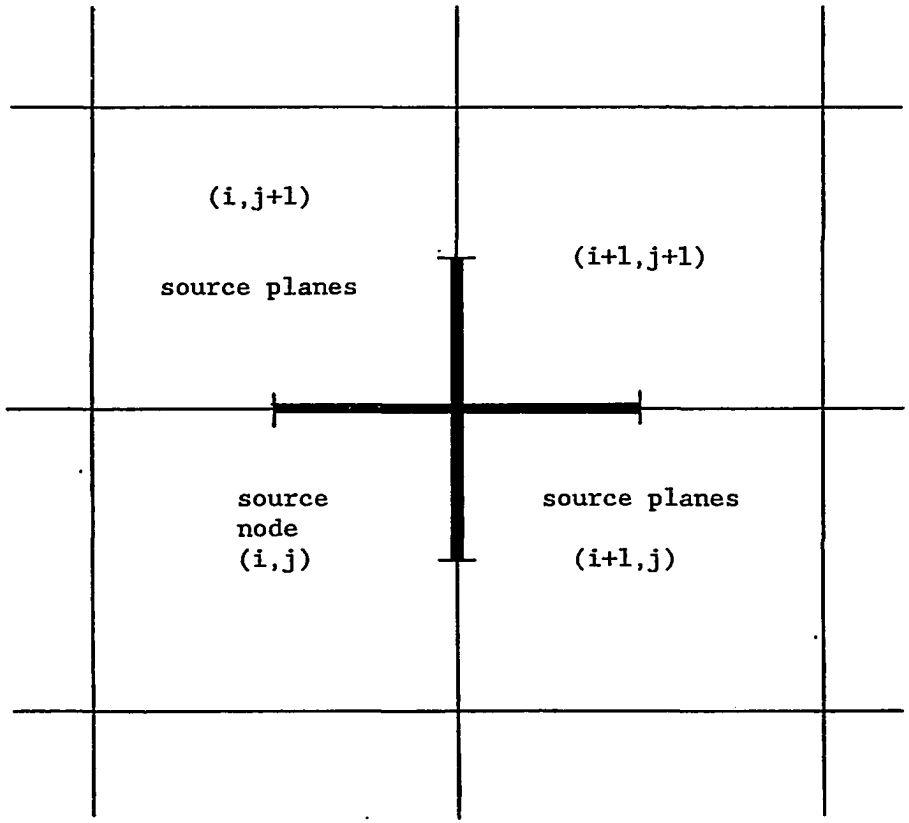

Figure 4.4. Source geometry for two-dimensional code

by the node (i,j) as shown in Figure 4.4.

In the case of a detector adjoint function, a real and an imaginary part of the fast flux and an imaginary part of the thermal flux are treated the same as the static flux calculation as explained above. But the real part of the thermal flux is evaluated using the Green's function condition at the source interface.

From Figure 4.4

$$D_{i,j}\frac{\partial\bar{\phi}_{i,j}}{\partial x} - D_{i+1,j}\frac{\partial\bar{\phi}_{i+1,j}}{\partial x} = S \qquad 4.42$$

$$D_{i,j+1}\frac{\partial\bar{\phi}_{i,j+1}}{\partial x} - D_{i+1,j+1}\frac{\partial\bar{\phi}_{i+1,j+1}}{\partial x} = S \qquad 4.43$$

$$D_{i,j}\frac{\partial\bar{\phi}_{i,j}}{\partial y} - D_{i,j+1}\frac{\partial\bar{\phi}_{i,j+1}}{\partial y} = S \qquad 4.44$$

$$D_{i+1,j}\frac{\partial\bar{\phi}_{i+1,j}}{\partial y} - D_{i+1,j+1}\frac{\partial\bar{\phi}_{i+1,j+1}}{\partial y} = S \qquad 4.45$$

where

D = Diffusion coefficient

$\bar{\phi}$ = Average flux at the interface from the previous iteration

and S is the source strength and has units of neutrons/cm^2-sec

Since the solutions of equations (4.42), (4.43), (4.44) and (4.45) will be parallel, only the flux from equation (4.42) will be developed. For simplicity, let

$$D(i,j) = D_p$$

$$\bar{\phi}(i,j) = \bar{\phi}_p$$

$$D(i+1,j) = D_q$$

$$\bar{\phi}(i+1,j) = \bar{\phi}_q$$

But at the interface

$$\bar{\phi} = \bar{\phi}_p = \bar{\phi}_q \qquad 4.46$$

Using the properties of the finite difference approximation, equation (4.42) will be

$$D_p\left(\frac{\bar{\phi} - \bar{\psi}_p}{\theta_p}\right) - D_q\left(\frac{\bar{\psi}_q - \bar{\phi}}{\theta_q}\right) = S \qquad 4.47$$

$$\bar{\phi} = \frac{S\theta_q\theta_p + D_p\theta_q\bar{\psi}_p + D_q\theta_p\bar{\psi}_q}{D_p\theta_q + D_q\theta_p} \qquad 4.48$$

The fluxes $\bar{\psi}_p$ and $\bar{\psi}_q$ are the average fluxes evaluated at some distance θ_p and θ_q respectively away from the node interface based on the respective node properties.

G. Convergence Criteria

The relaxation method as described in reference (31) can be used for the polynomial nodal model to speed up the convergence as

$$\bar{\phi}^{(k)} = \bar{\phi}^{(-k)}w + (1-w)\bar{\phi}^{(k-1)} \qquad 4.49$$

where

$\bar{\phi}^{(k-1)}$ = Average value from the previous iteration, (k-1)

$\bar{\phi}^{(-k)}$ = Average value evaluated for the current iteration (k)

$\bar{\phi}^{(k)}$ = New updated average value to be used in the evaluation of constants for iteration (k)

w = The Relaxation parameter

k = Iteration number

The speed of convergence will depend on the relaxation parameter, w. If the relaxation parameter, w, is greater than unity, it is called over-relaxation and if it is less than unity, it is called under-relaxation. The relaxation method was applied to the following parameters:

1. The coefficients of the polynomial, e.g.,

$$a_{ij}^{(k)} = a_{ij}^{(-k)}w + (1-w)a_{ij}^{(k-1)} \qquad 4.50$$

2. The average flux at the interface conditions

$$\bar{\phi}^{(k)} = \bar{\phi}^{(-k)}w + (1-w)\bar{\phi}^{(k-1)} \qquad 4.51$$

3. The neutron source

$$S^{(k)} = S^{(-k)}w + (1-w)S^{(k-1)} \qquad 4.52$$

where

$$S = \frac{\sum_{i=1}^{N}\left(\sum_{g=1}^{G}\nu\Sigma_{fg}\bar{\phi}_g\right)\Delta v_i}{\sum_{i=1}^{N}\Delta v_i} \qquad 4.53$$

i = Number of node

g = Energy group in node i

N = Total number of nodes

G = Total number of energy groups

Δv = Volume of node i

$\bar{\phi}$ = Average flux of energy group g in node i

Benghanam (32) found that the interface relaxation parameter governed the oscillation of the eigenvalue. He also suggested that the interface relaxation parameter should be under relaxed to prevent the oscillation at low iteration numbers and that the source relaxation parameter should be over relaxed in order to increase the convergence of the system. He derived a set of relaxation parameters which were used to speed up the convergence process. For this dissertation, these values were used. No attempt was made to obtain a new set of relaxation parameters for the convergence enhancement.

At the end of each iteration the convergence value was calculated using the following equation

$$\epsilon = \frac{\left[\dfrac{\sum_{i=1}^{N} \sum_{g=1}^{G} \left(1 - \dfrac{\bar{\phi}_{i,g}^{(k)}}{\bar{\phi}_{i,g}^{(k-1)}}\right)^2 \Delta v_i}{\sum_{i=1}^{N} \Delta v_i} \right]^{\frac{1}{2}}}{NG} < 1.E\text{-}8 \qquad 4.54$$

where

ϵ = Error term of the flux between two iterations

G = Number of energy group

$\bar{\phi}$ = Average flux of energy group g in node i

N = Number of nodes

Δv = Volume of node

k = Iteration number

V. ANALYSIS OF RESULTS

A. Analysis of Results of the One-Dimensional Two-Energy Group Computer Code

A one-dimensional two-energy neutron group computer program was developed to calculate the static flux and the frequency dependent real and imaginary detector adjoint functions based on the polynomial nodal technique as explained in Chapters III and IV. The flux in each node is defined by a fourth order polynomial. This computer code is called ONED2G. A flow chart of ONED2G is given in Figure 5-1.

The steady state fast and thermal fluxes were calculated using ONED2G for the Iowa State University UTR-10 reactor. The cross sections used in the solutions were those calculated by Al-Ammar (11) and Huang and Danofsky (23) and are listed in Table 5.1. The nodalization used for the UTR-10 to calculate an eigenvalue using the ONED2G code is shown in Figure 5-2. The thermal flux calculated using ONED2G is plotted as shown in Figure 5-3. The eigenvalue, K_{eff}, obtained using ONED2G is 0.9994 which is 0.1% less than the value obtained using the analytical solution (11).

The real and imaginary components of the detector adjoint function for the UTR-10 reactor were calculated using ONED2G. The nodalization used to calculate the Green's function for the UTR-10 reactor is shown in Figure 5.4. The Green's function was calculated for a frequency of 10 rad/sec. A frequency of 10 rad/sec. was chosen because it is within

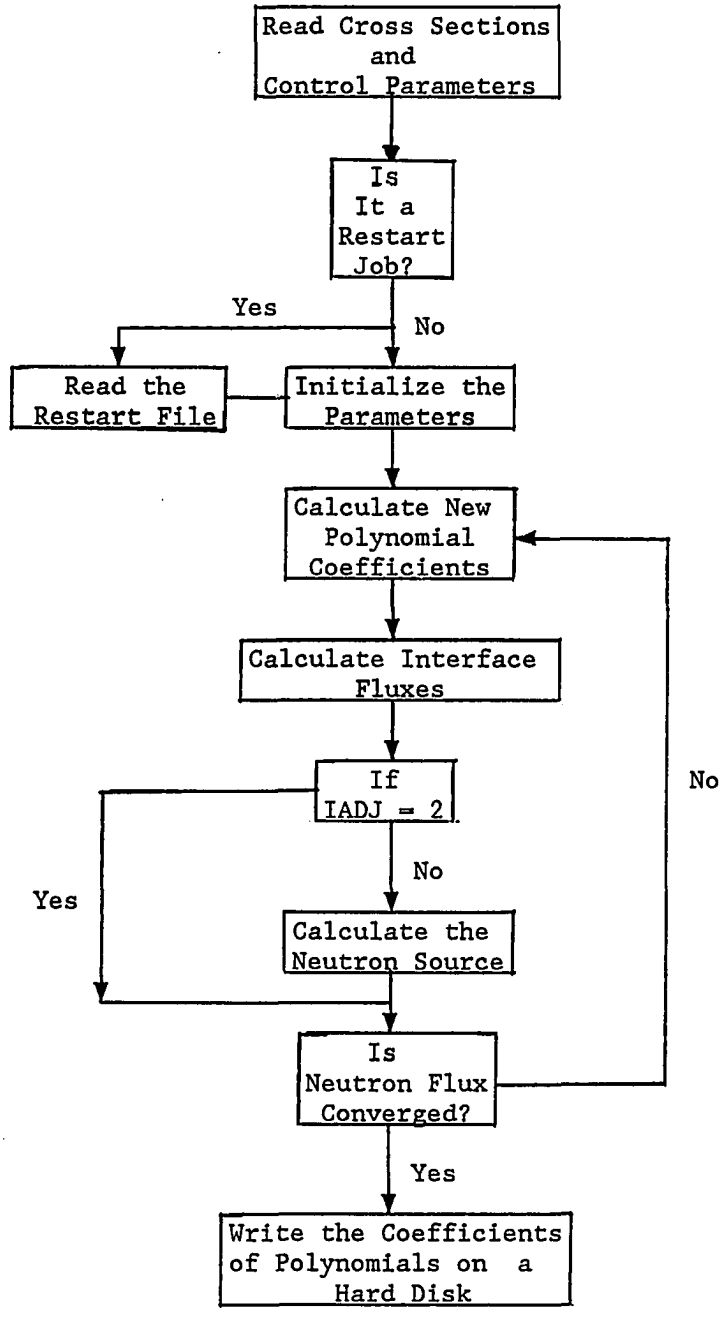

Figure 5.1. Flow chart used in the nodal model computer codes

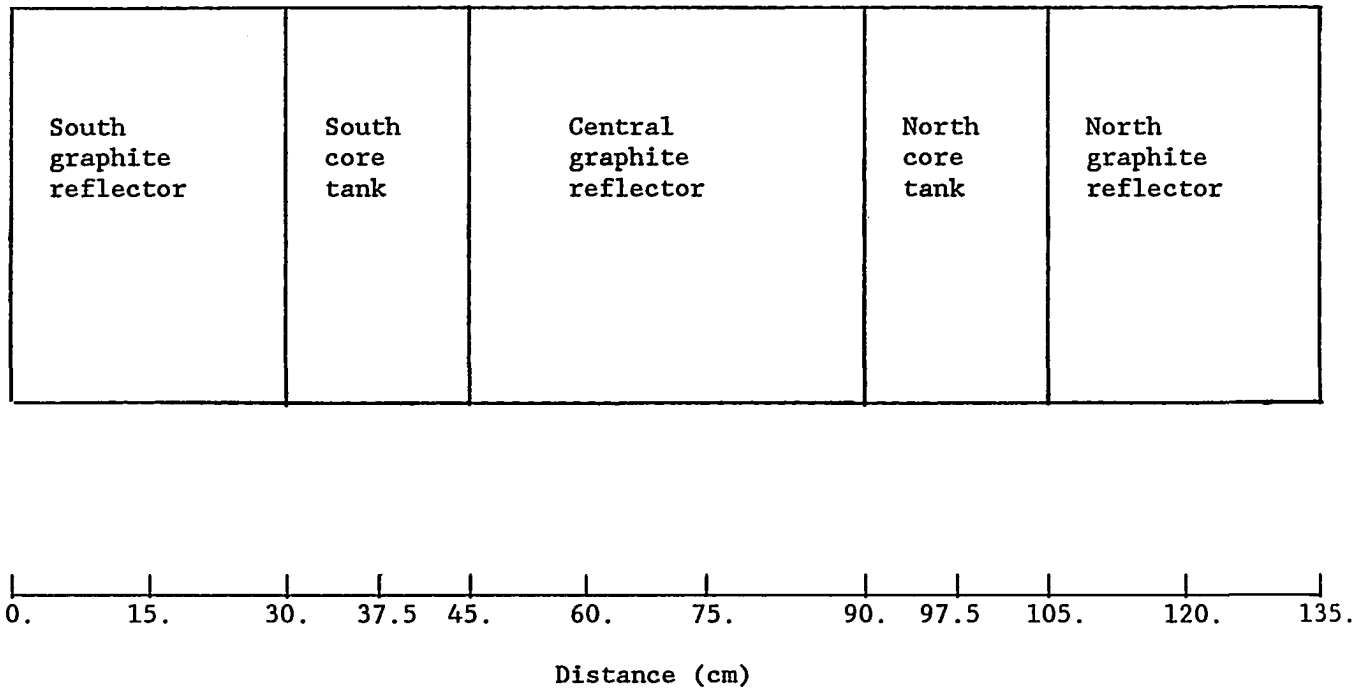

Figure 5.2. One-dimensional geometry of the UTR-10 reactor used in eigenvalue calculation

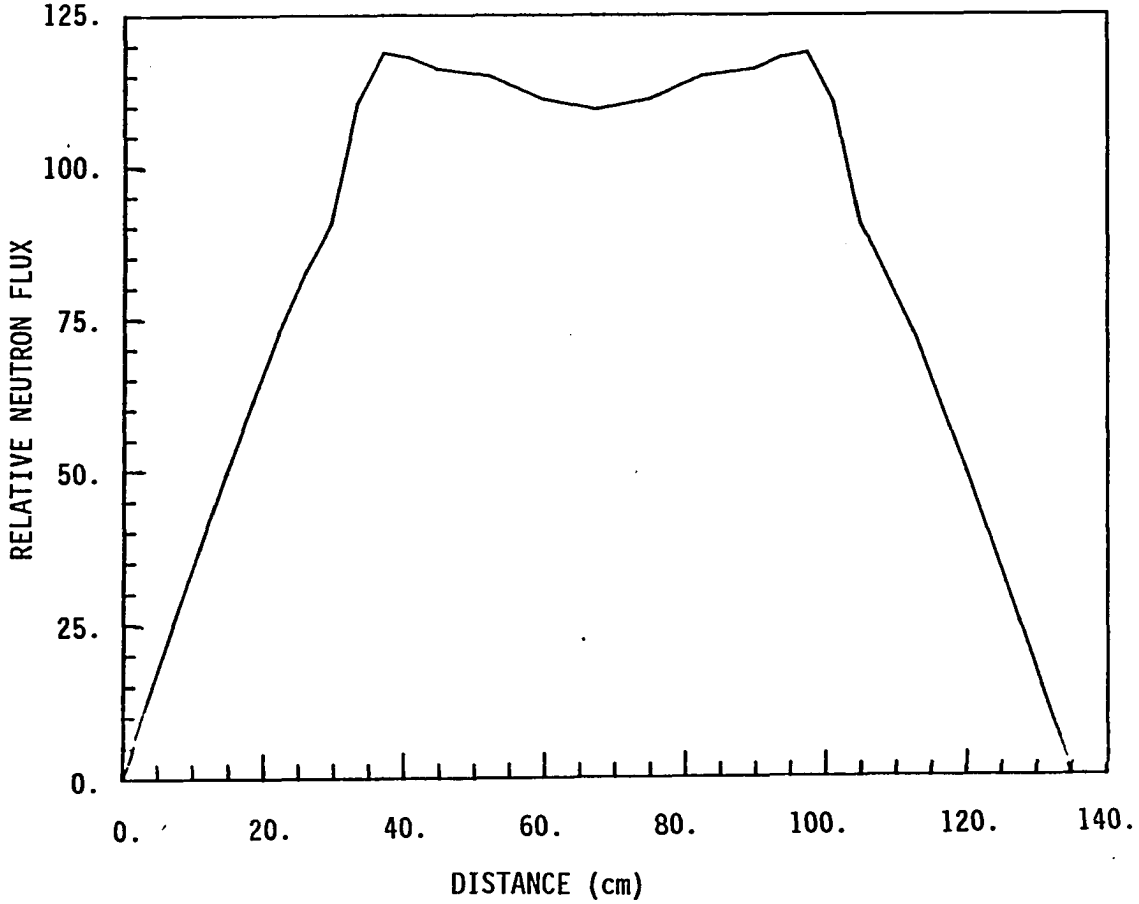

Figure 5.3. UTR-10 thermal flux profile by a one-dimensional computer code

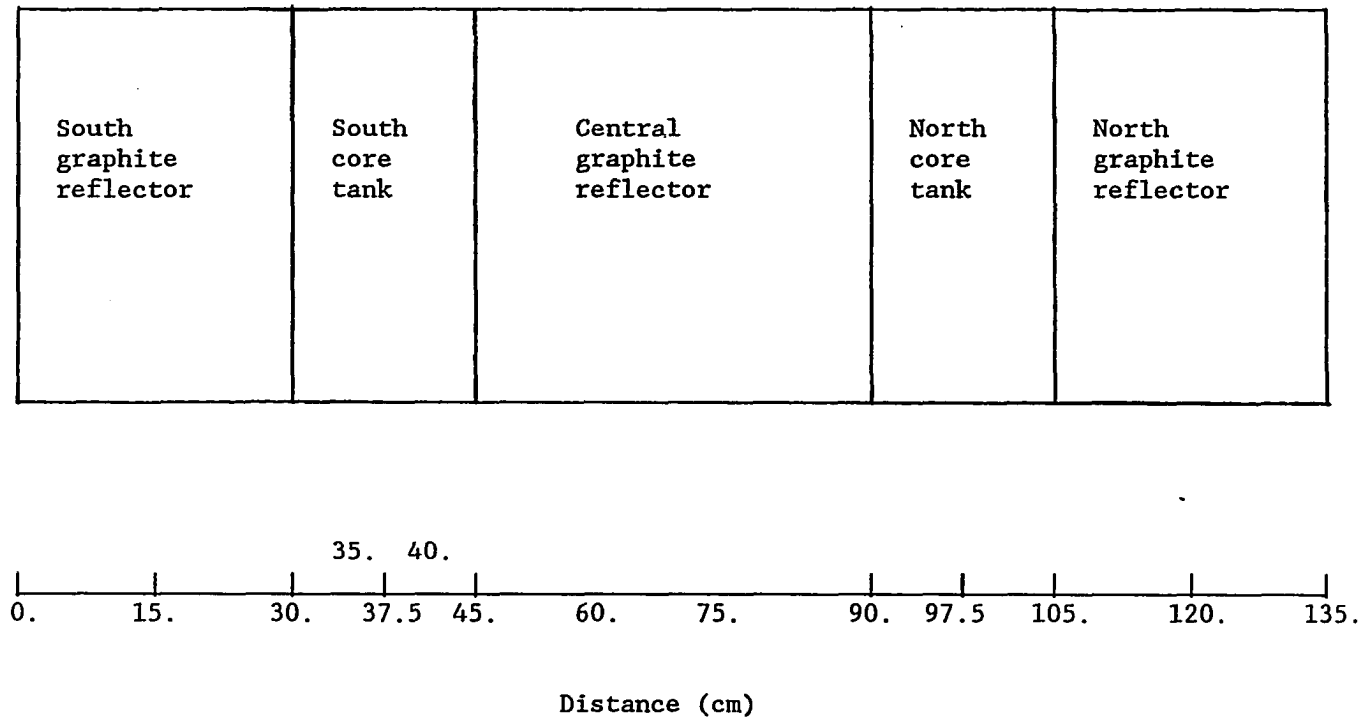

Figure 5.4. One-dimensional geometry of the UTR-10 reactor used in Green's function calculation

the plateau region of the global response, i.e., the zero power transfer function. The detector was positioned at 37.5 cm, in the middle of the south fuel tank region. Figure 5.5 presents a comparison of the detector adjoint functions obtained from the analytical solution and the nodal model method solution. It was expected that the perturbation located in the fuel region will generate a higher amplitude signal compared to the signal generated in the graphite region. This is obviously due to the neutron multiplication process in the fuel region which amplifies the signal. The real thermal detector adjoint function obtained using the ONED2G code peaked approximately 2% higher near the detector region compared to the analytical solution (11).

The currents at both sides of the node interface were calculated using the polynomials of the respective node. As expected from the required continuity of currents, the currents on both sides of the node were within $\pm$ 0.5% of the average value at the interface. The difference of the derivatives at the source was 2% higher than the input value of 1.

The phase angle of the detector adjoint function obtained using the ONED2G code and the analytical solution (11) are compared in Figure 5.6. The phase angle is defined as the arctangent of the ratio of the imaginary to real parts of the detector adjoint function. The phase angle varies from a minimum of -3.33 to a maximum of -3.41 rad. As expected, the relative value of the imaginary component compared to the

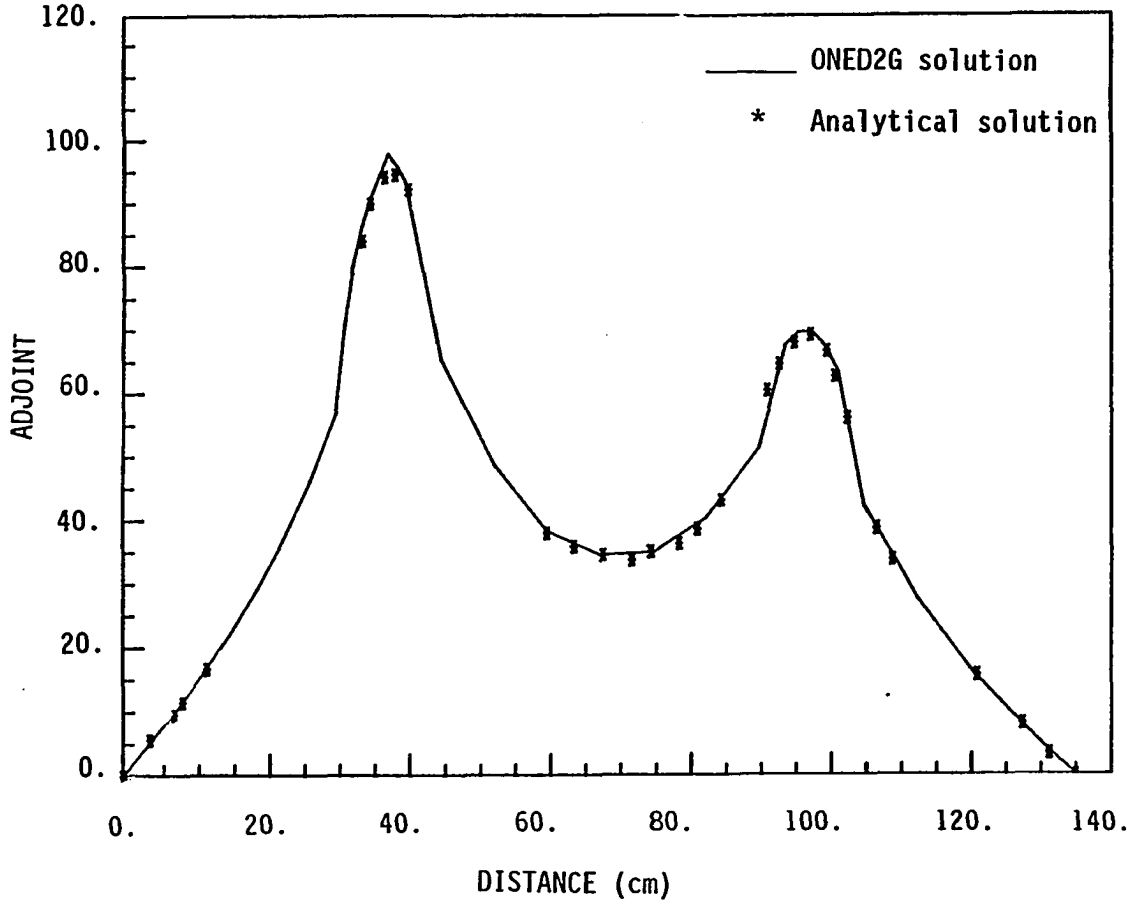

Figure 5.5. Comparison of thermal detector adjoint function for detector location at 37.5 cm in UTR-10

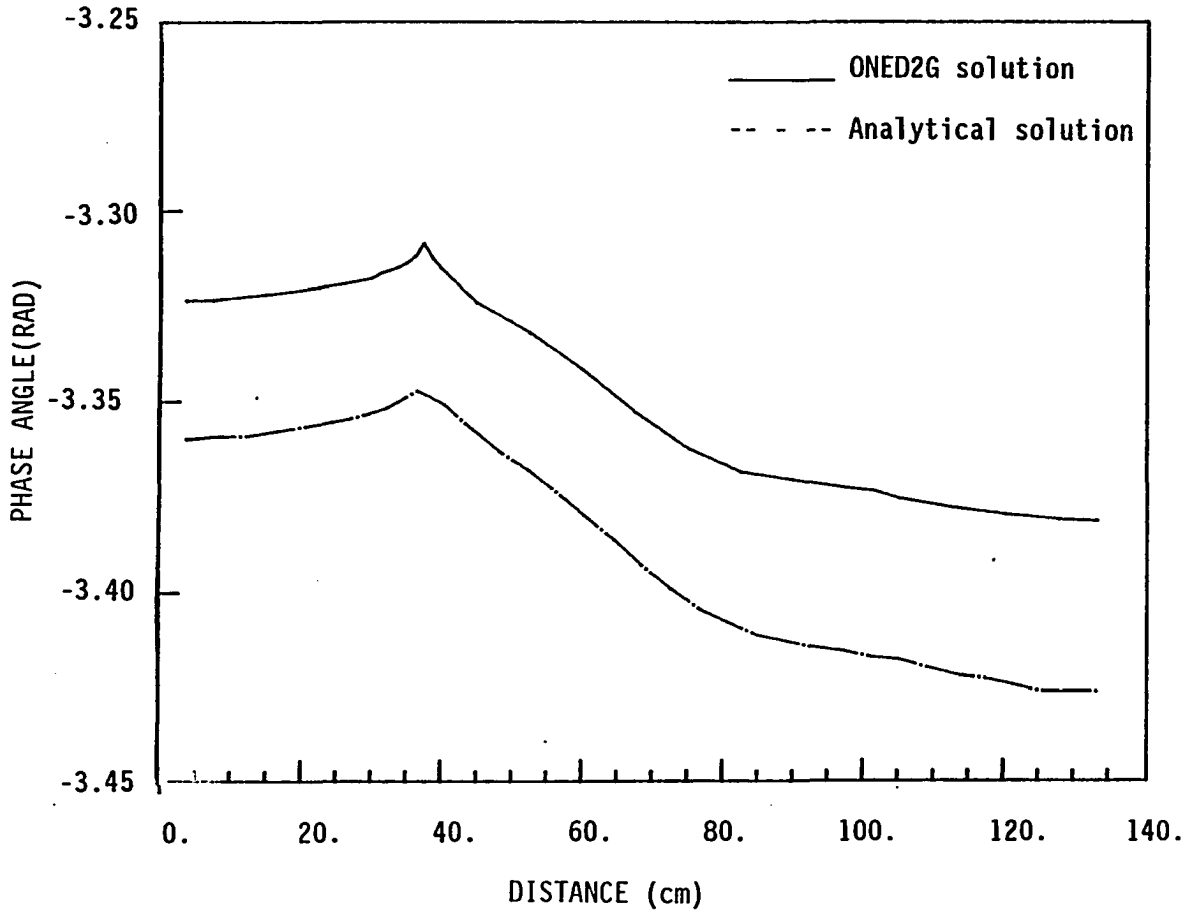

Figure 5.6. Comparison of the detector adjoint function phase for the detector location at 37.5 cm in UTR-10

real component of the detector adjoint function gets smaller as the detector location is approached. The absolute value of the phase angles are greater than 180 degrees. This is because the perturbation term $\delta\Sigma_a$ is taken as positive rather than negative as used by Pazsit and Analytis (13) in the development of the Green's functions. The phase angles obtained using the ONED2G code were within 2% of the values obtained using the analytical solution (11). An enlarged scale for the phase angle in Figure 5.6 is used to illustrate the shape.

B. Analysis of Results of the Two-Dimensional One-Energy Group Computer Code

A computer code TWOD1G was developed to calculate the one-energy group static flux and the frequency dependent real and imaginary detector adjoint function. The flow chart of the TWOD1G code is similar to the flow chart for the ONED2G code. The TWOD1G computer code was benchmarked against the EXTERMINATOR computer code (12) and the analytical solution. One energy group cross section data were obtained from Duderstadt and Hamilton (14) and are listed in Table 5.2. A reactor size of 200 cm x 200 cm was chosen.

In the EXTERMINATOR computer code (12), a node size smaller than the diffusion length is recommended. Since the diffusion length is on the order of 4 to 5 cm, a large number of nodes will be required. Therefore, a diffusion coefficient was arbitarily chosen such that the diffusion length did not exceed the maximum node size of 20 cm. This

reduced the size of the problem to be executed using the EXTERMINATOR computer code. No such restrictions are applicable to the nodal model technique.

An eigenvalue problem for a 200 cm x 200 cm homogenous subcritical reactor was executed. The eigenvalue; K_{eff}, calculated by TWOD1G was 0.8557 which is .01% less than the eigenvalue of 0.8558 obtained from an analytical solution. The nodalization used to perform the eigenvalue calculation using TWOD1G is as shown in Figure 5.7. The coefficients of the polynomials obtained for each node were stored in a file so they could be used later to calculate the static flux as a function of position.

The detector adjoint function for this subcritical homogenous reactor was calculated using TWOD1G. The nodalization used to obtain the Green's function using TWOD1G is shown in Figure 5.8. The heavy lines in Figure 5.8 represents the source planes. A frequency of 10 rad/sec was chosen because it is within the plateau region of the global response, i.e., the zero power transfer function. The source, 10 cm x 10 cm, was positioned at the center of the core (100 cm, 100 cm). Figures 5.9 and 5.10 are the surface plots of the real and imaginary detector adjoint function obtained from TWOD1G. The thermal detector adjoint function peaked at the source as expected.

Using the EXTERMINATOR code, the real part of the detector adjoint function was calculated at several locations along the center of the core. Similarly, using equation (3.25); an analytical solution for the

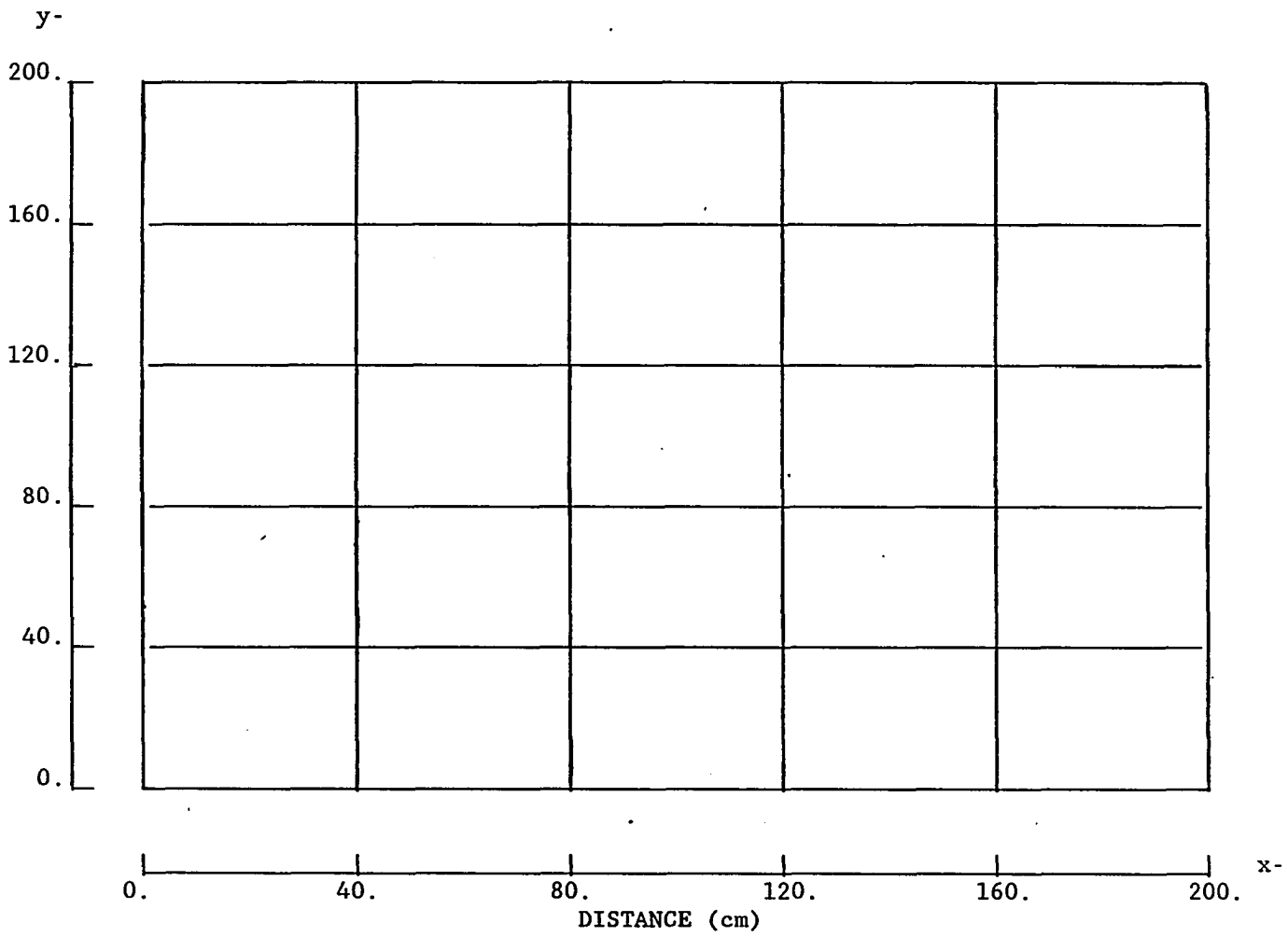

Figure 5.7. Nodal geometry of homogenous (200 cm x 200 cm) reactor used in eigenvalue calculation

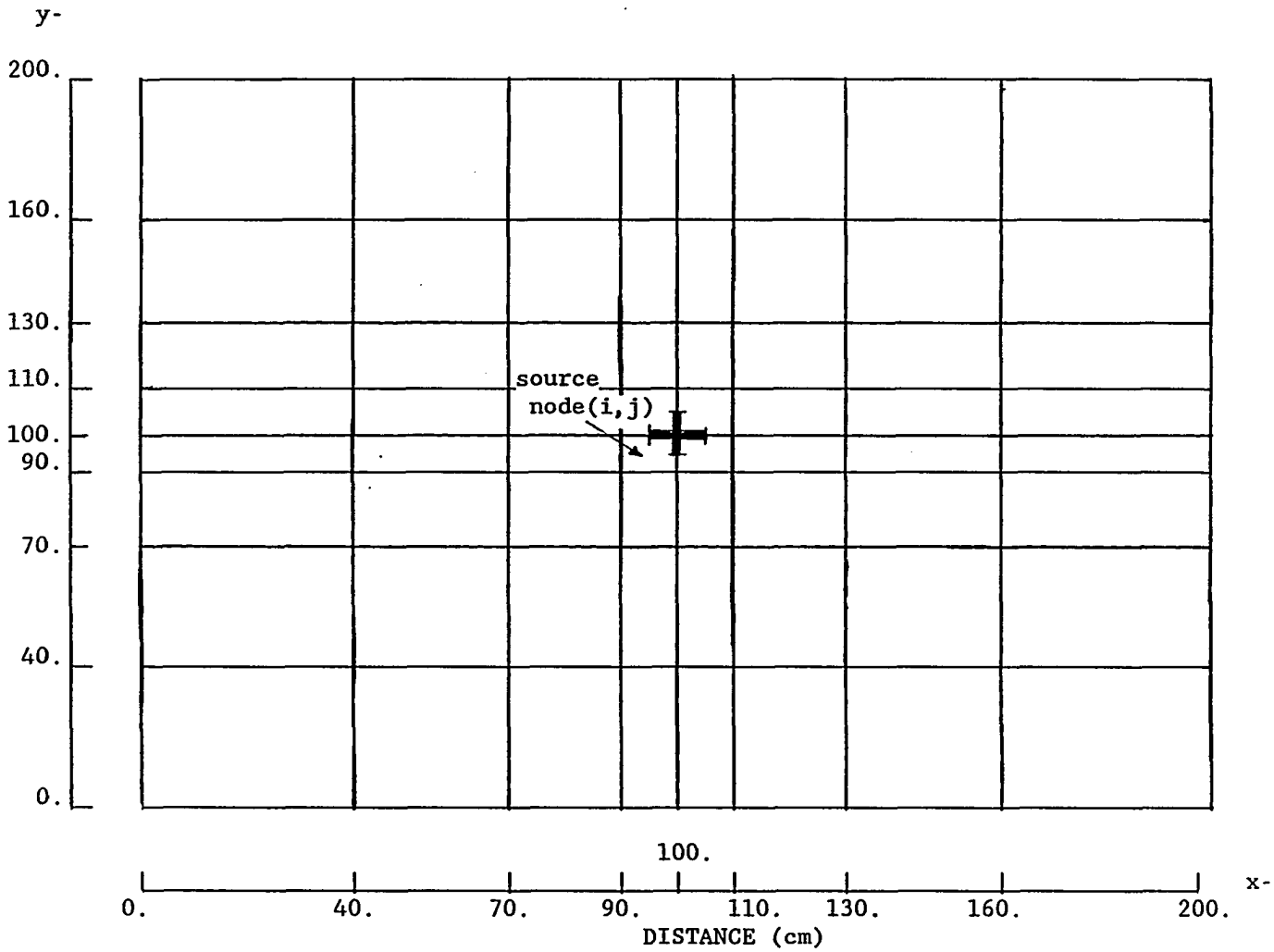

Figure 5.8. Nodal geometry of homogenous (200 cm x 200 cm) reactor used in Green's function calculation

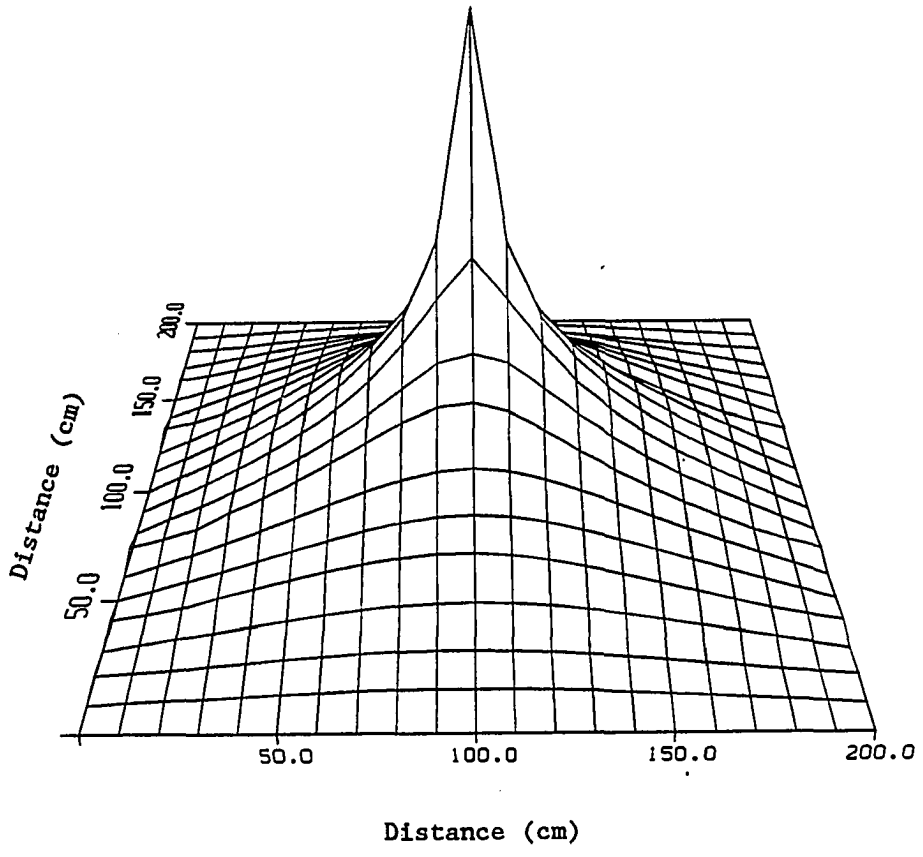

Figure 5.9. Surface plot of the real detector adjoint function for the detector located in the center of the homogenous (200 cm x 200 cm) reactor

Negative of the imaginary detector adjoint function

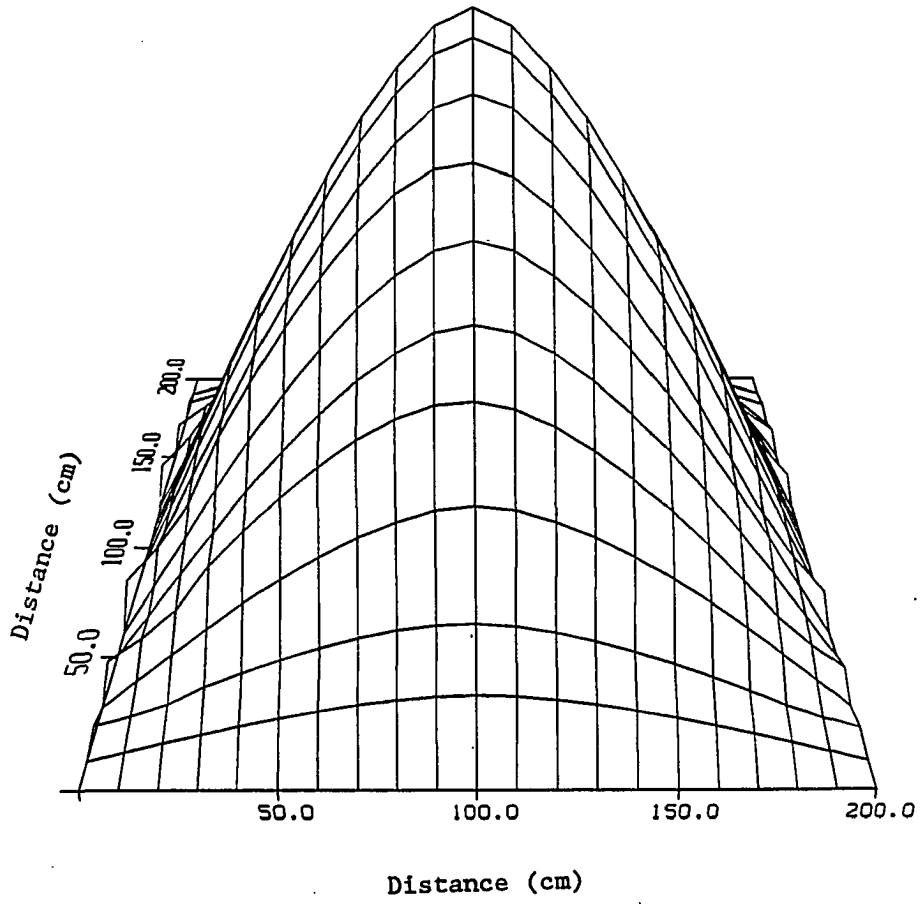

Figure 5.10. Surface plot of the imaginary detector adjoint function for the detector located in the center of the homogenous (200 cm x 200 cm) reactor

detector adjoint function; $\psi(x_d, x_p, y_d, y_p, \omega)$, was calculated for the same locations. The values obtained from the analytical solution and from the EXTERMINATOR computer code were within 1% of each other.

The detector adjoint function obtained using TWOD1G was normalized to the values obtained from the analytical solution and is plotted as shown in Figure 5.11 across the core at y=100 cm. The values obtained using TWOD1G were found to be less than 1% greater at 20 cm away from the source region and about 3% greater closer to the source compared to the analytical solution and the values obtained from the EXTERMINATOR code.

The average value of neutron current based on the polynomials on the left node of the interface and the average value of current based on the right node of the interface are calculated by the code. The currents at the interface matched within 1% of the average value at the interface. Figure 5.12 shows the continuity of the current of the real component of the detector adjoint function across the core in the y direction at various x-locations. Figure 5.13 shows the discontinuity in current at the detector position. No discontinuity in the current was observed in the case of the imaginary component of the detector adjoint function.

Using the GPLOT computer code, as shown in equation (3.6), x- and y- components of the detector response and the phase angles at several core locations were calculated. The GPLOT computer code was developed to calculate the detector response using the coefficients of the

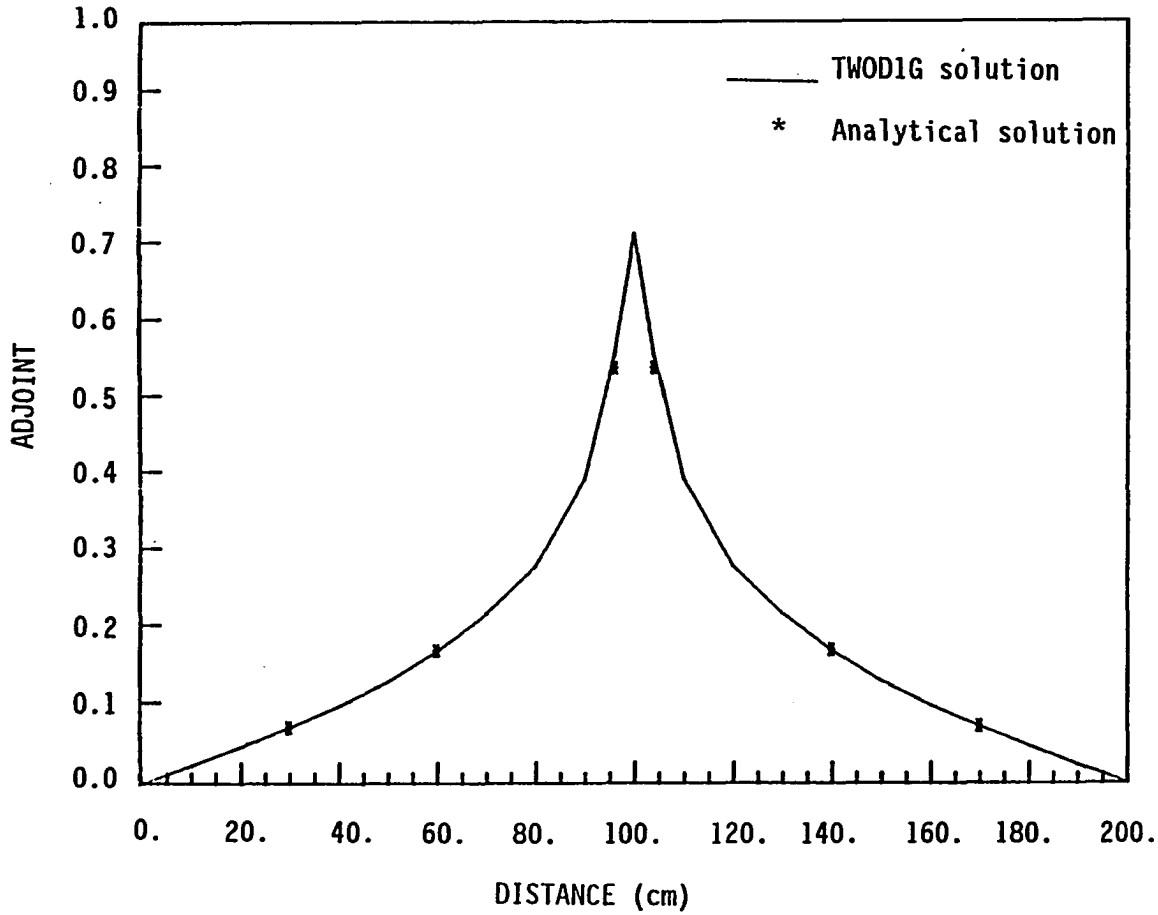

Figure 5.11. Comparison of the real detector adjoint function for the detector location in the center of the homogenous (200 cm x 200 cm) reactor

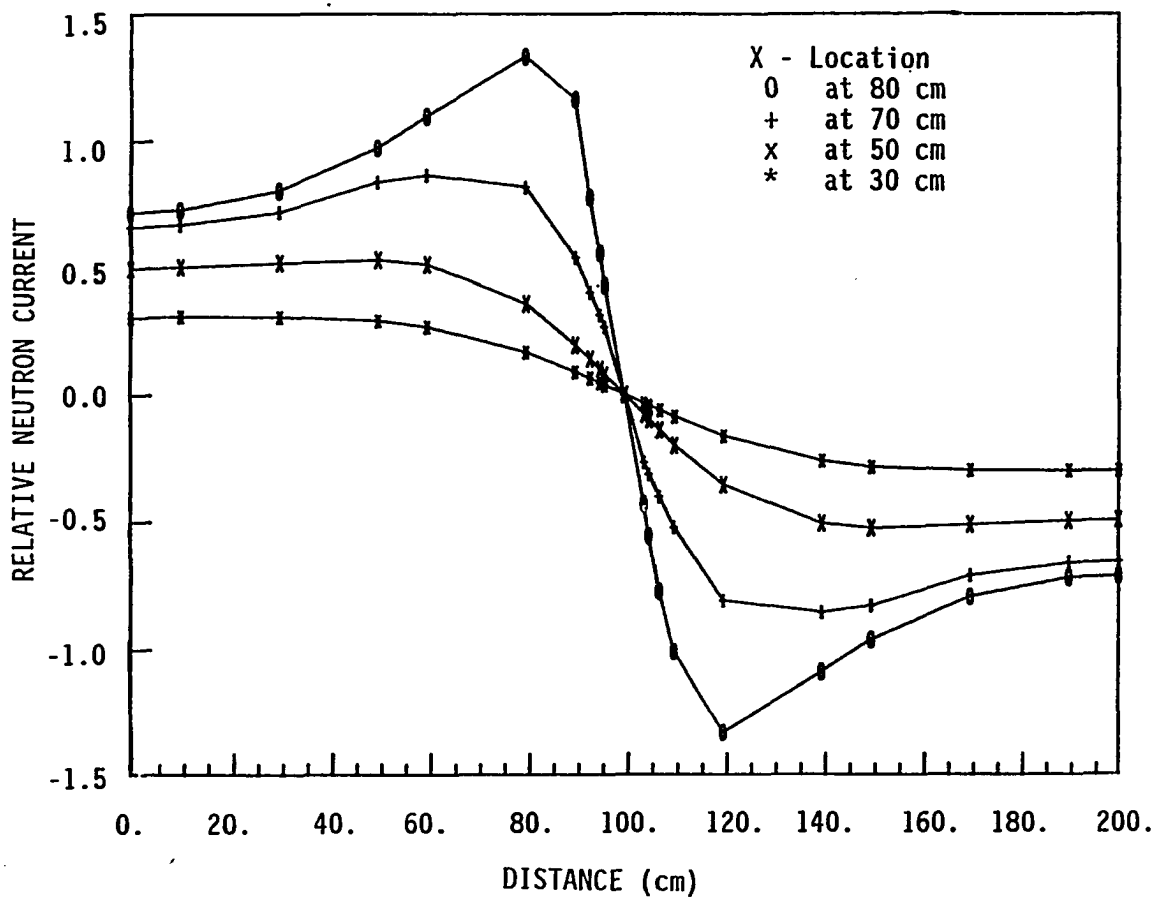

Figure 5.12. Neutron current across the core in y-direction at various x-locations for the detector location in the center of the homogenous (200 cm x 200 cm) reactor

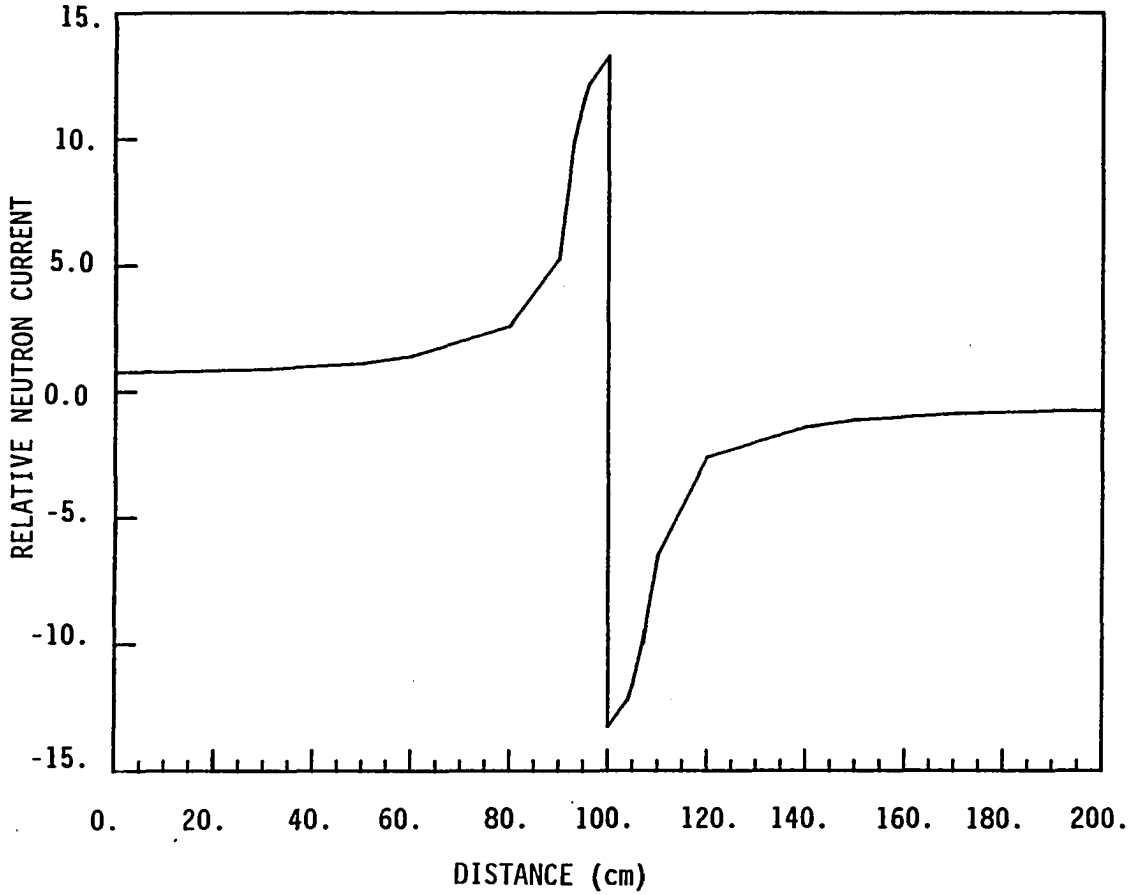

Figure 5.13. Neutron current through the center of core in y-direction for the detector location in the center of the homogenous (200 cm x 200 cm) reactor

polynomial for the static flux and the detector adjoint function generated by the TWOD1G computer code. GPLOT also calculates the current in the x- and y- directions for the static flux as well as the real and the imaginary parts of the detector adjoint function. The phase angle is calculated as the arctangent of the ratio of the imaginary to the real parts of the solution. The quadrant of the phase angle can be determined from the positive or negative sign of the real and the imaginary part.

The detector adjoint function for the 8 cm x 8 cm source located in the center of this reactor was calculated using TWOD1G. The values of the detector adjoint function obtained were smaller by a factor of 0.8, compared to the values obtained for the same reactor using a 10 cm x 10 cm source located in the center of the core. The later problem required a larger number of iterations to converge. As the source size was reduced further, a convergence problem was encountered.

C. Analysis of Results of the Two-Dimensional Two-Energy Group Computer Code

The computer code TWOD1G was modified to calculate the two-energy group static flux and the frequency dependent real and imaginary detector adjoint function. This computer code is called TWOD2G. The flow chart of TWOD2G is similar to the flow chart for ONED2G.

The code was benchmarked against the EXTERMINATOR computer code using the two-energy group cross sections for the UTR-10 reactor as listed in Table 5.3. The nodalization used to perform an eigenvalue calculation using TWOD2G is shown in Figure 5.14. The eigenvalue; K_{eff}, of 1.003 obtained using TWOD2G is within 0.05% the value obtained using the EXTERMINATOR computer code. The solution for the thermal-flux, calculated by the computer code TWOD2G and the EXTERMINATOR computer code, across the reactor (from south to north) along the center line of the reactor is shown in Figure 5.15. The relative value of the thermal flux in the UTR-10 reactor calculated by the TWOD2G computer code was within 1% of the value calculated by EXTERMINATOR.

An eigenvalue problem was executed using a 60 cm x 60 cm subcritical homogenous reactor. Two-energy group cross sections, as listed in Table 5.4, were obtained from the ANL benchmarked cross section data book (33). The nodalization used to perform the eigenvalue calculation using the TWOD2G code is shown in Figure 5.16. From the TWOD2G computer code, the eigenvalue of the reactor was found to be 0.8596 which is 0.05% higher compared to the value of 0.8593 obtained from the analytical solution.

The detector adjoint function was calculated for a frequency of 10 rad/sec using a 6 cm x 6 cm source positioned in the center of the core. The nodalization diagram used to calculate the detector adjoint function is shown in Figure 5.17. The heavy lines in Figure 5.17

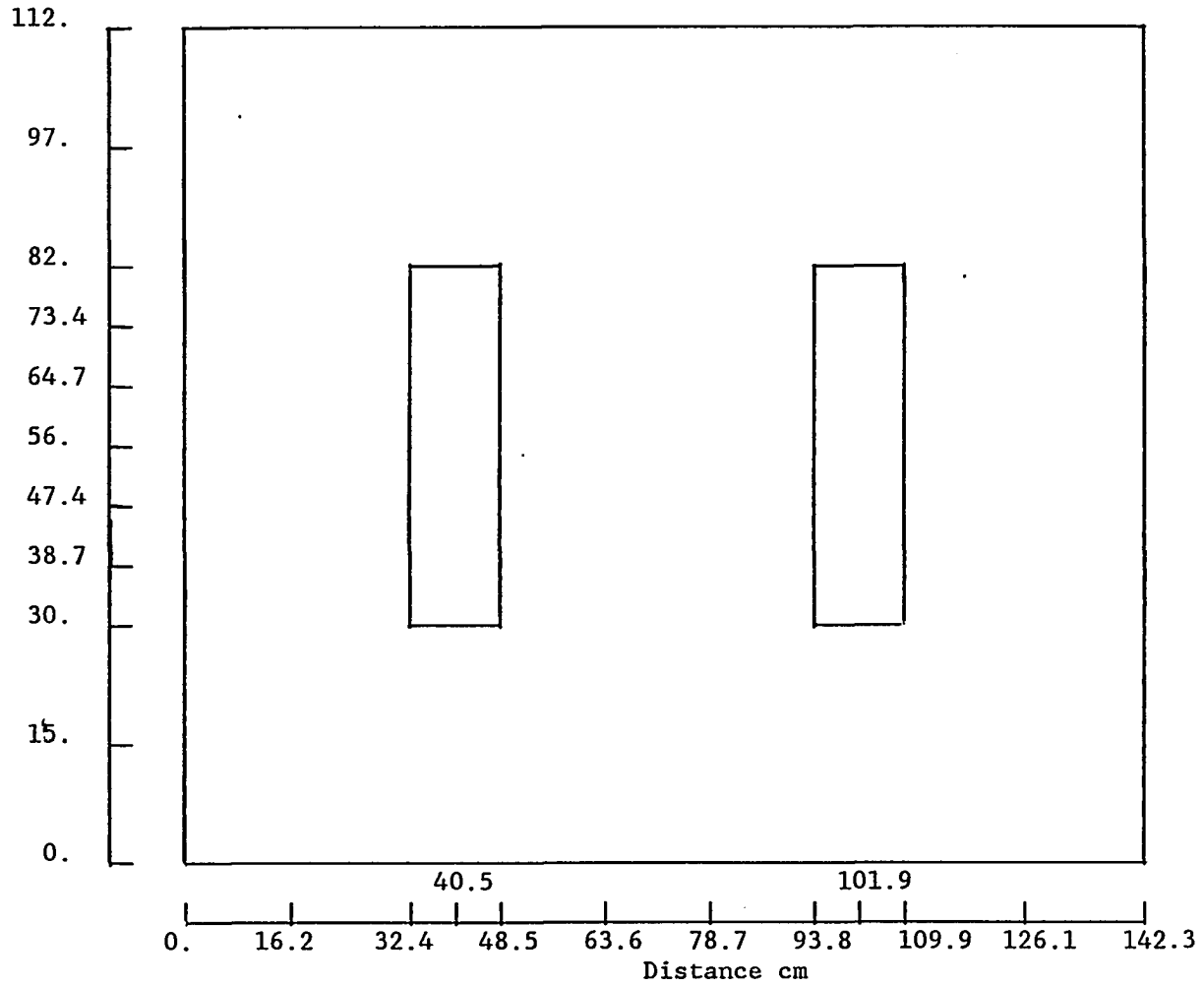

Figure 5.14. Two-dimension geometry of the UTR-10 reactor used in eigenvalue calulation

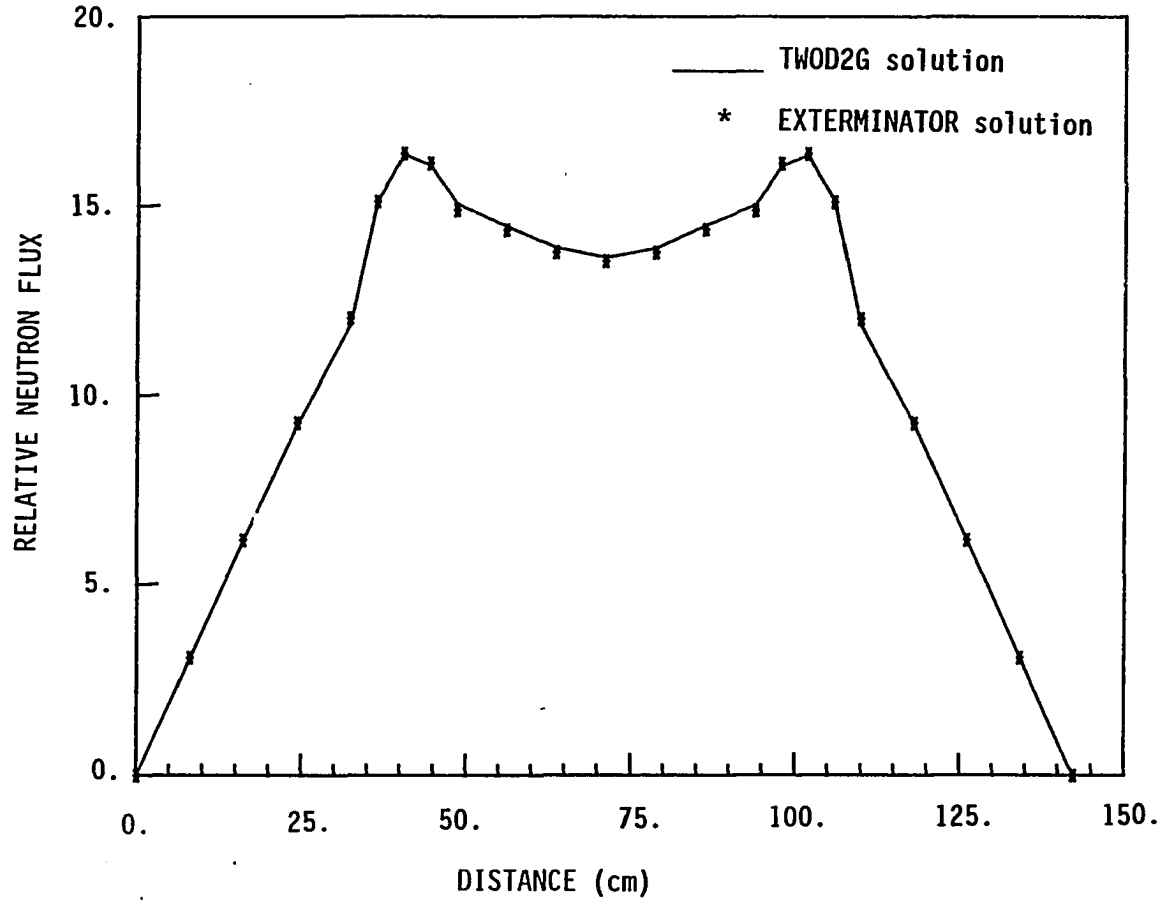

Figure 5.15. Comparison of thermal flux across the UTR-10 reactor at y = 56.5 cm

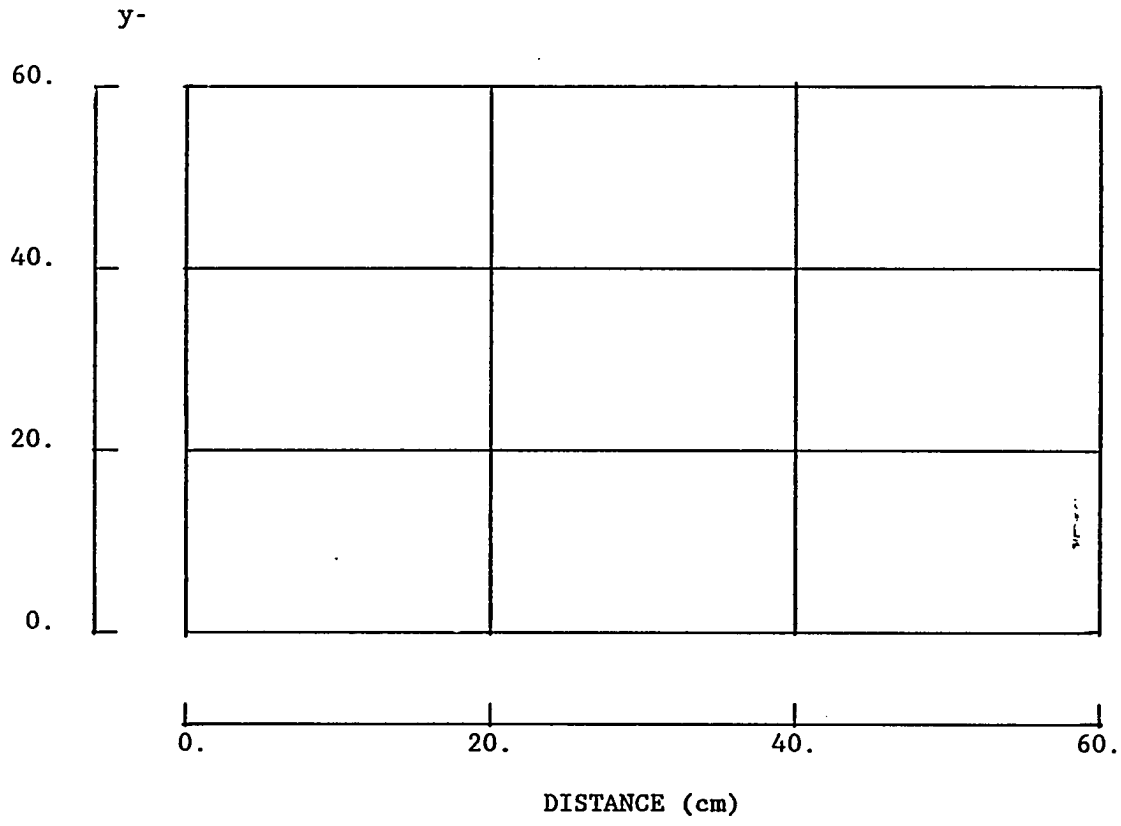

Figure 5.16. Nodal geometry of homogenous (60 cm x 60 cm) reactor used in eigenvalue calculation

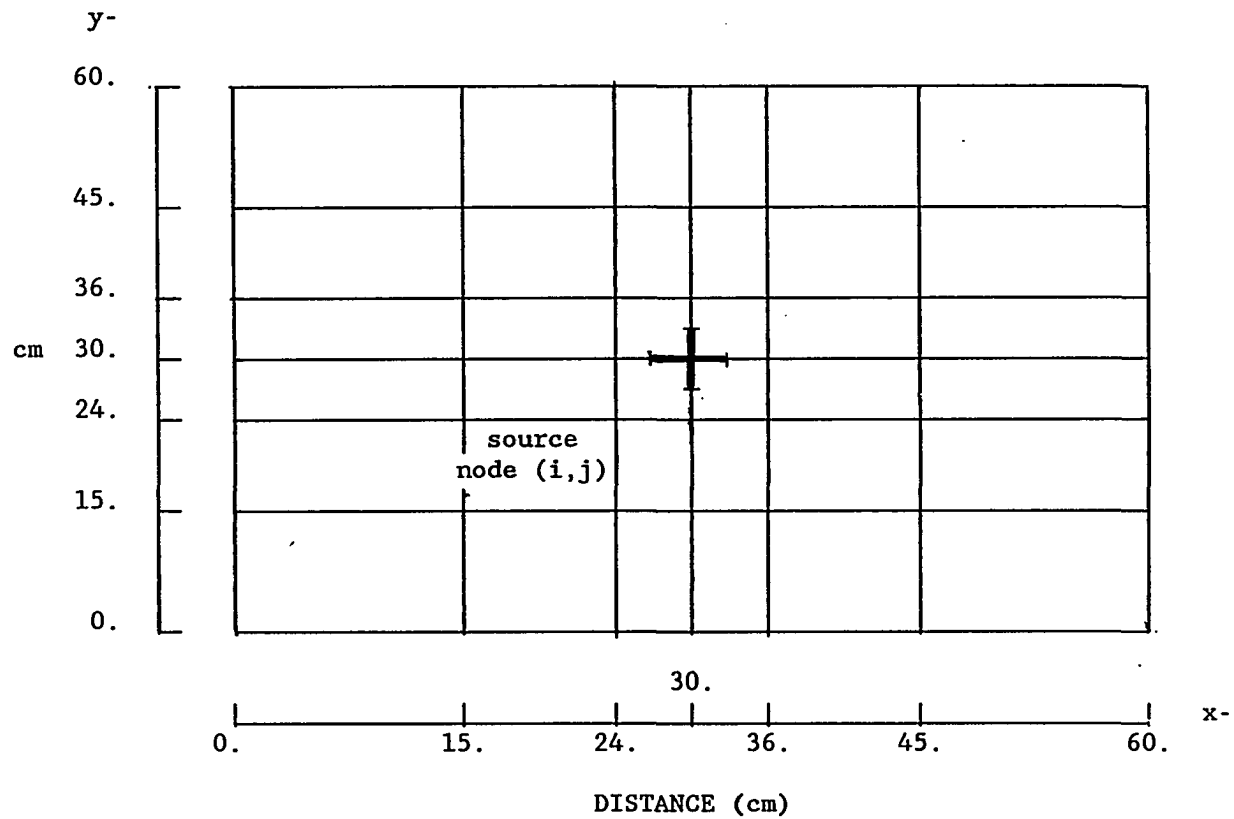

Figure 5.17. Nodal geometry of homogenous (60 cm x 60 cm) reactor used in Green's function calculation

represent the source planes. The thermal detector adjoint function peaked in the center as shown in Figure 5.18. The real and imaginary components of the fast detector adjoint function are shown in Figures 5.19 and 5.20. The imaginary thermal detector adjoint function is plotted in Figure 5.21.

The average current based on the polynomials on the left node of the interface and the average value of current based on the right node of the interface are calculated by the code. The currents of the real components of the detector adjoint function at the interface matched within 1% of the average value at the interface. Figure 5.22 shows the continuity of the current of the real thermal detector adjoint function across the core in the y direction at various x-locations. Figure 5.23 shows the discontinuity in the current of the real thermal detector adjoint function at the detector position as expected.

The current of the imaginary fast and thermal detector adjoint function on both sides of the interface varied $\pm$ 2% from the average value at the interface. No discontinuity in the current was observed in the case of the fast real and imaginary and thermal imaginary components of the detector adjoint function at the detector location.

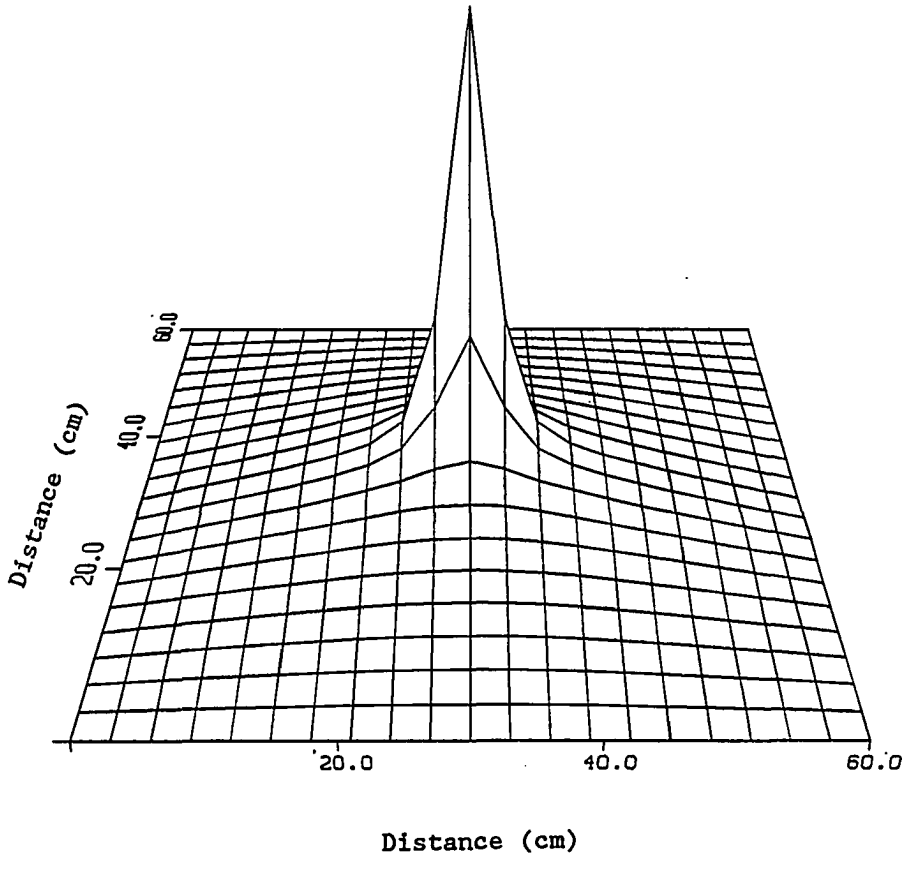

Figure 5.18. Surface plot of the thermal real detector adjoint function for the detector located in the center of the homogenous (60 cm x 60 cm) reactor

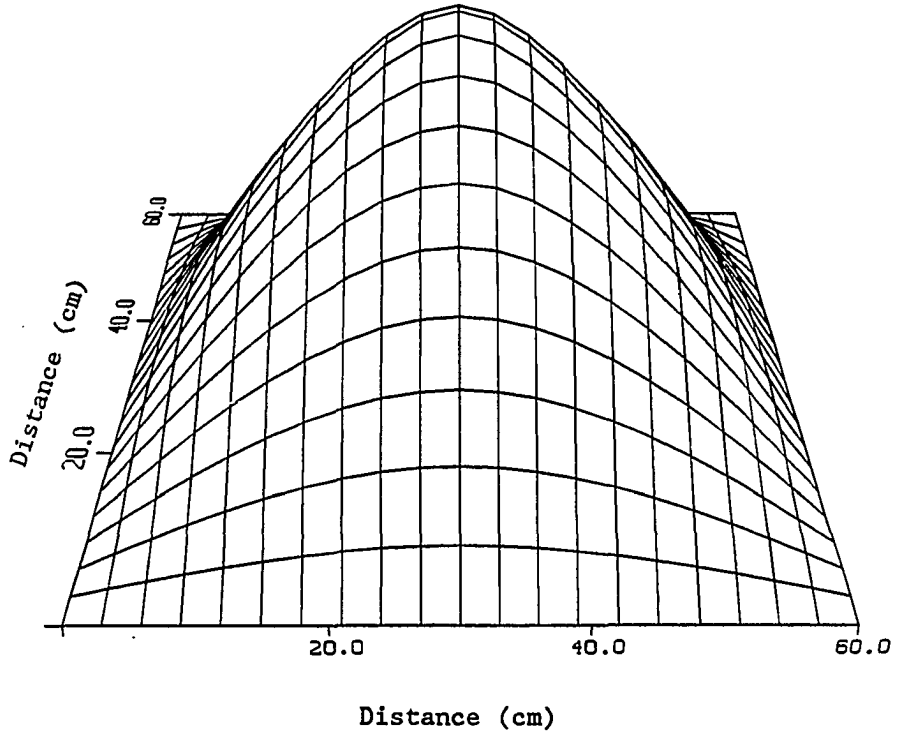

Figure 5.19. Surface plot of the fast real detector adjoint function for the detector located in the center of the homogenous (60 cm x 60 cm) reactor.

Negative of the imaginary detector adjoint function

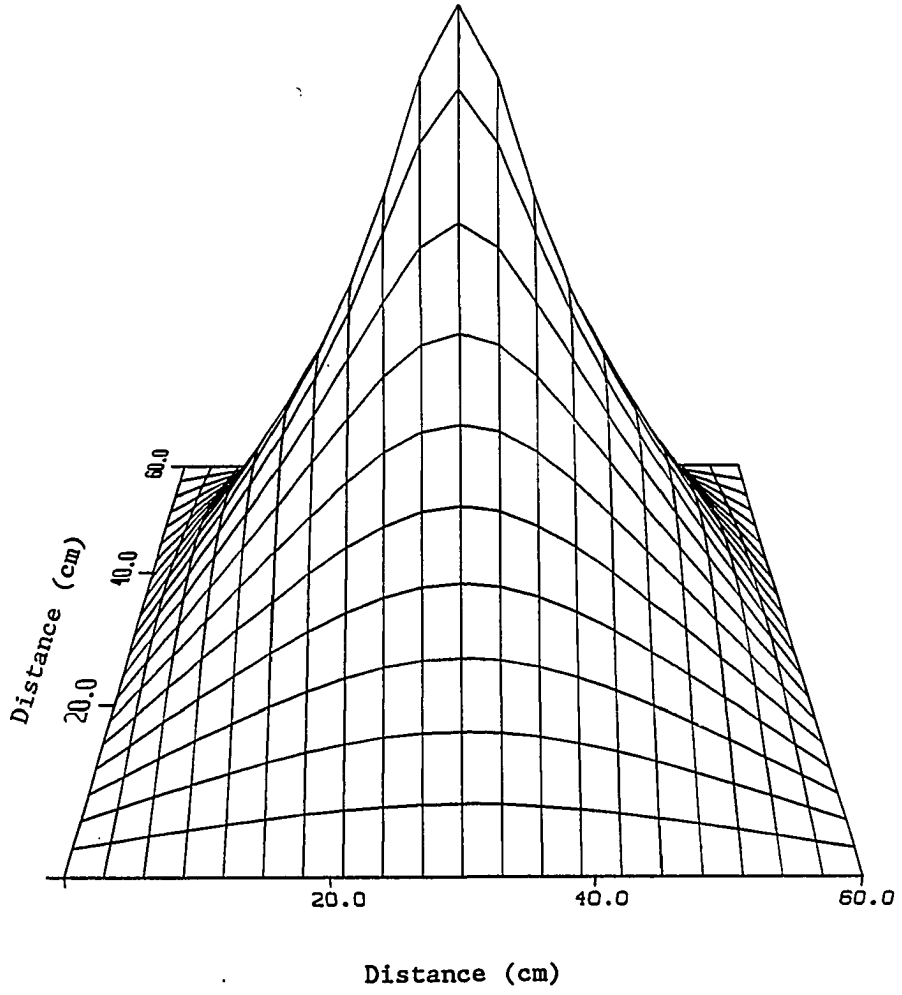

Figure 5.20. Surface plot of the fast imaginary detector adjoint function for the detector located in the center of the homogenous (60 cm x 60 cm) reactor

Negative of the imaginary detector adjoint function

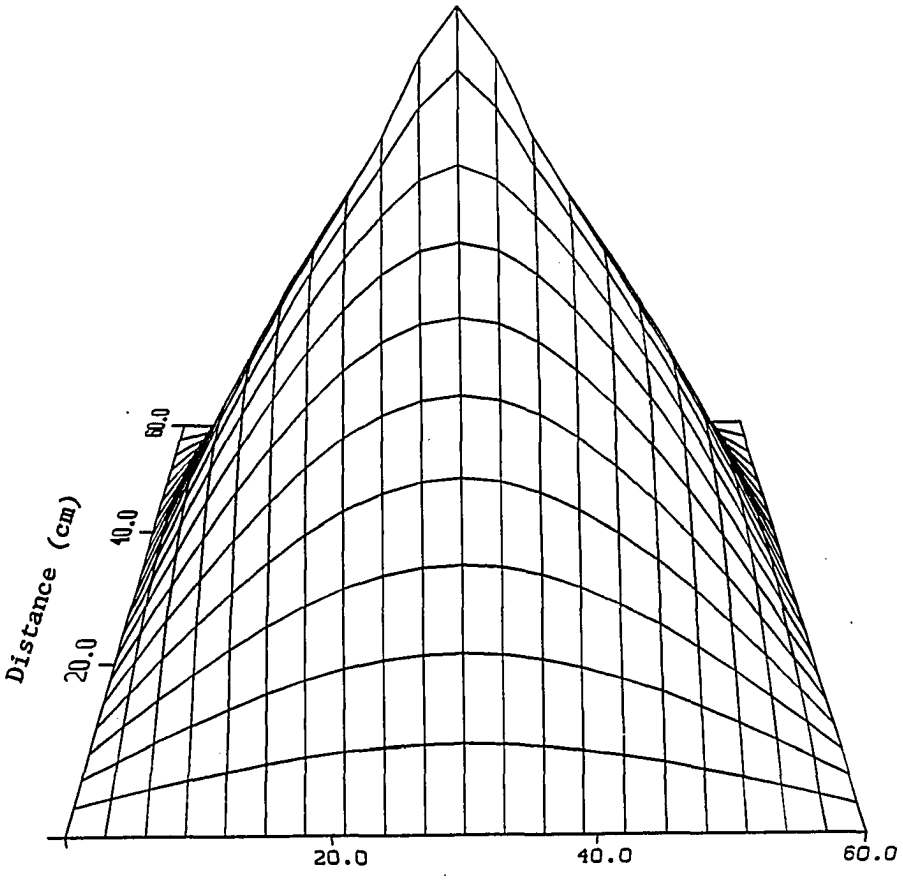

Figure 5.21. Surface plot of the thermal imaginary detector adjoint function for the detector located in the center of the homogenous (60 cm x 60 cm) reactor

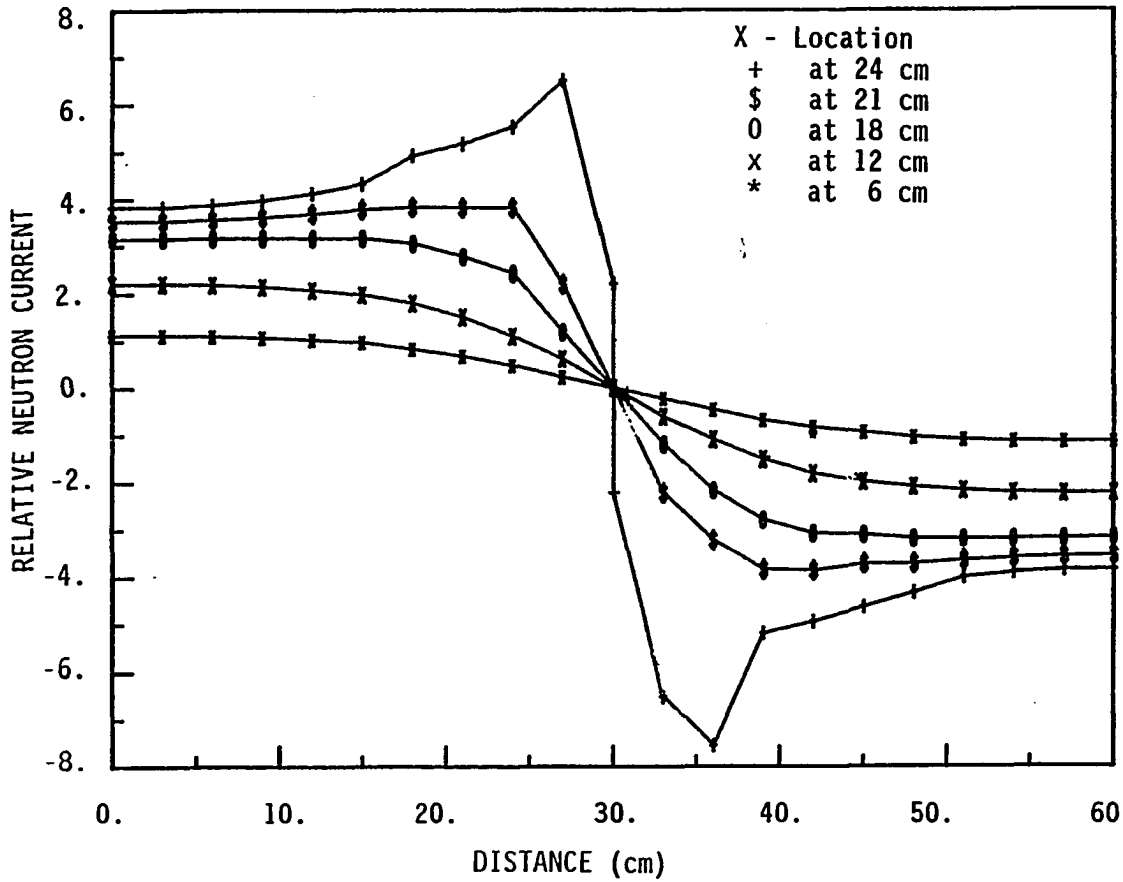

Figure 5.22. Neutron current across the core in y-direction at various x-locations for the detector located in the center of the homogenous (60 cm x 60 cm) reactor

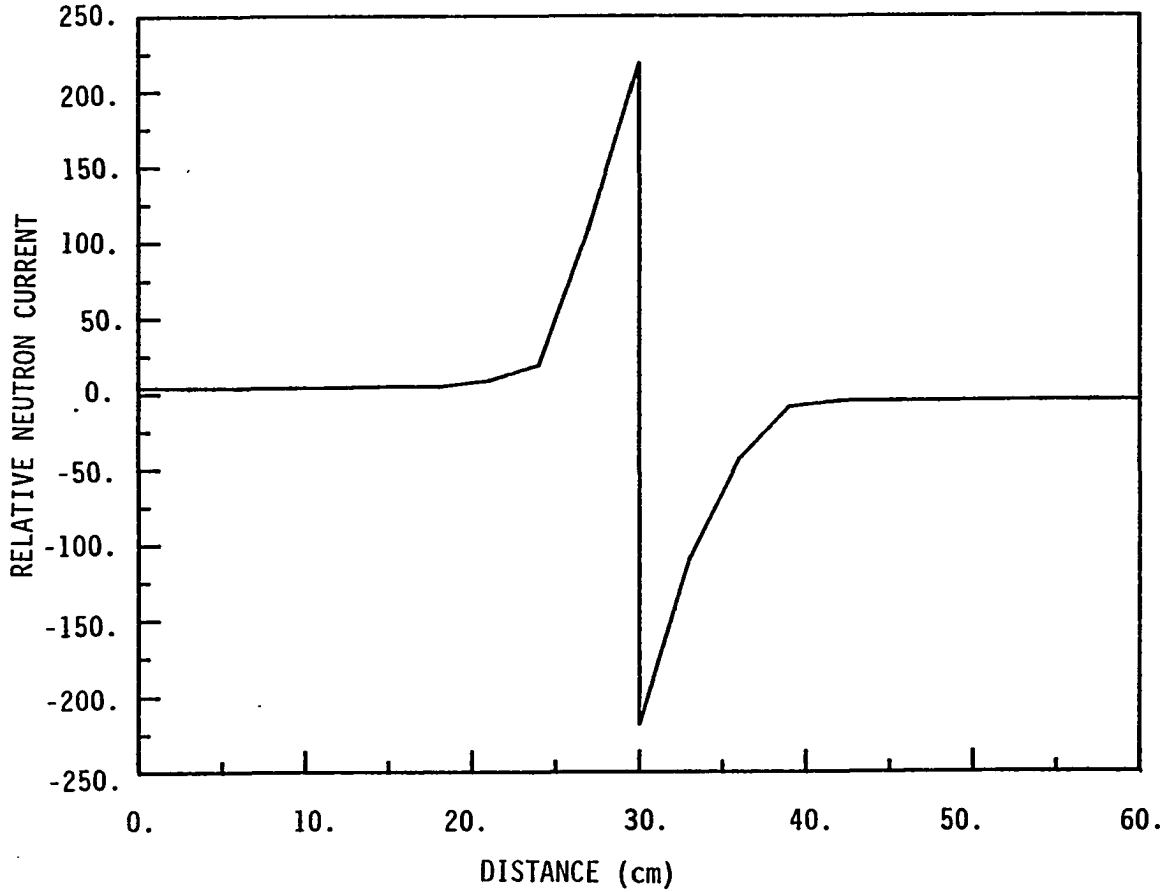

Figure 5.23. Neutron current through the center of core in y-direction for the detector located in the center of the homogenous (60 cm x 60 cm) reactor

The phase angle for the frequency of 10 rad/sec was calculated using the zero power transfer function which is shown by Uhrig (15) as follows:

$$G_R = \frac{\left[\frac{\ell}{1-K}\right]\left[j\frac{\omega}{\lambda} + 1\right]}{\left[\frac{j\omega}{\left(\frac{1-K(1-\beta)}{\ell}\right)}\right]\left[\frac{j\omega}{\left(\frac{\lambda(1-k)}{1-K(1-\beta)}\right)} + 1\right]} \qquad 6.1$$

where

ℓ = neutron life time, sec

The Neutron life time, ℓ, is calculated using the following equation, as shown by Duderstadt and Hamilton (14)

$$\ell = \left(\frac{1}{1 + L^2B^2}\right)\left(\frac{1}{\Sigma_a v_2}\right) \qquad 6.2$$

where

L^2 = Diffusion Area, cm^2

$$= \frac{D}{\Sigma_a}$$

B^2 = Geometric buckling, cm^{-2}

$$= \left(\frac{\pi}{a}\right)^2 + \left(\frac{\pi}{b}\right)^2$$

where a and b are the dimensions of the reactor. Substituting the value of a, b, Σ_a, v_2 and d in the equation (6.2) yields

$\ell = 5.5 \times 10^{-5}$ sec

Substituting the value of ℓ, B^2, K, and ω the phase angle of the zero power point reactor will be 0.2 degrees.

The phase angle calculated by the TWOD2G computer codes varied from 0.2 degrees near the source to 0.4 degrees away from the source. These values are well within the range of the phase angle value calculated using the zero power transfer function.

Table 5.1

Cross section parameters for the one-dimensional UTR-10 reactor geometry

Energy Group	D cm	Σ_a cm-1	$\nu\Sigma_f$ cm-1	Σ_{1-2} cm-1	Trans. Buckling
Fuel Region					
1-Fast	1.4214	.19626E-2	.18663E-2	.34129E-1	.216E-2
2-Thermal	.23158	.52410E-2	.76407E-1		.216E-2
Graphite Region					
1-Fast	1.1529	.53263E-8	0.	.28736E-2	.216E-2
2-Thermal	.99181	.30661E-4	0.		.216E-2

One-group delayed neutron fraction β = .0065

Decay constant = 0.1 sec^{-1}

Table 5.2

Cross section parameters for the homogenous (200 cm x 200 cm) reactor

Energy Group	D cm	Σ_a cm-1	$\nu\Sigma_f$ cm-1	Σ_{1-2} cm-1	Trans. Buckling
1-Thermal	61.3	.1532	.157	.34129E-1	0.

One-group delayed neutron fraction β = .007

Decay constant = 0.1 sec^{-1}

Table 5.3

Cross section parameters for the two-dimensional

UTR-10 reactor geometry

Energy Group	D cm	Σ_a cm-1	$\nu\Sigma_f$ cm-1	Σ_{1-2} cm-1	Trans. Buckling
Fuel Region					
1-Fast	1.406	.1976E-2	0.	.3425E-1	.11E-2
2-Thermal	.2230	.5339E-1	.7802E-1		.11E-2
Graphite Region					
1-Fast	1.165	0.	0.	.2526E-2	.11E-2
2-Thermal	.9915	.2013E-3	0.		.11E-2

One-group delayed neutron fraction β = .0065

Decay constant = 0.1 sec^{-1}

Table 5.4

Cross section parameters for the homogenous

(60 cm x 60 cm) reactor

Energy Group	D cm	Σ_a cm-1	$\nu\Sigma_f$ cm-1	Σ_{1-2} cm-1	Trans. Buckling
1-Fast	1.5	.01	0.2	0.	0.
2-Thermal	.4	.08	.135	0.	0.

One-group delayed neutron fraction β = .0065

Decay constant = 0.1 sec^{-1}

VI. CONCLUSIONS

The purpose of this research was to investigate the applicability of a polynomial nodal model technique to the calculations of the real and the imaginary parts of the detector adjoint function. Models were developed using one-dimensional two-energy neutron groups, two-dimensional one-energy neutron group and two-dimensional two-energy neutron groups approximations. It has been demonstrated that the static flux and the complex detector adjoint function as well as the detector response can be obtained as a function of position using nodal techniques. From the analysis of the results as discussed in Chapter V, it is concluded that the nodal model technique can be used to calculate the detector adjoint function and the phase angle.

The phase angle and the magnitude of the detector adjoint functions for a frequency of 10 rad/sec were calculated using the two-energy group computer code ONED2G for a neutron detector located in the middle of the south core tank of the Iowa State University UTR-10 reactor in one-dimensional geometry. The real detector adjoint function obtained using the OND2G code peaked approximately 2% higher near the detector region compared to the values obtained from the analytical solution. The currents on both sides of the node interface were within $\pm$ 0.5% of the average value at the interface. The phase angles were within 2% of the values obtained from the analytical solution.

Using the one-energy group computer code TWOD1G, the magnitude of the frequency dependent detector adjoint function and the phase angle were calculated for the detector located in the center of a 200 cm x 200 cm homogenous reactor. The real part of the detector adjoint function was compared with the results obtained from the EXTERMINATOR computer code as well as the analytical solution based on a double sine series expansion using the classical Green's Function solution. The values were found to be less than 1% greater at 20 cm away from the source region and about 3% greater closer to the source compared to the values obtained from the analytical solution and the EXTERMINATOR code. The currents at the node interface matched within 1% of the average value at the interface. The phase angle varied from 0.1 degrees to 0.4 degrees compared to 0.2 degrees calculated using the point reactor zero power transfer function.

A computer code TWOD2G was used to solve for the two-energy group detector adjoint function and the phase angle for the detector located in the center of a 60 cm x 60 cm homogenous reactor. An analytical solution based on a double sine series expansion using the classical Green's functions solution was developed. It was found that a large number of terms in the series were required for convergence, and in some cases(near the source) convergence was not possible for even a very large number of terms. The result seems to follow the expected

behavior of the Green's functions, however. The phase angle calculated using TWOD2G varied from 0.2 degrees to 0.4 degrees compared to 0.2 degrees calculated using the point reactor zero power transfer function.

VII. SUGGESTIONS FOR FUTURE WORK

The following recommendations are suggested to improve the nodalization model technique:

1. A set of relaxation parameters developed by Benghanam (32) was used in this study. An algorithm needs to be developed to enhance the convergence of the system.
2. A criterion needs to be developed for a selection of the node size. From a sensitivity study of the node size, it was found that for convergence of the system, a fewer number of iterations were required when the node sizes near the boundary were kept large compared to the node size at the center. Similarly, a criterion needs to be developed to determine the source plane size for the source location away from the center.
3. An application of the nodal model method to a three-dimensional problem needs to investigated.
4. From the analysis of results, it was found that the average currents of the imaginary parts of the adjoint function did not match as well as the average currents of the real parts of the detector adjoint function at the interface. A better technique for convergence criteria needs to be developed.

VII. REFERENCES

1. J. C. Robinson, Analysis of neutron fluctuation spectra in the Oak Ridge Research Reactor and the High Flux Isotope Reactor, Report ORNL-4149 (1967).

2. S. E. Stephenson, D. P. Roux, and D. N. Fry, Neutron fluctuation spectra in the Oak Ridge research reactor, Report ORNL-TM-1401 (1966).

3. A. Lucia, E. Ohlmer and D. Schwalm, Correlation between neutron noise and fuel element oscillation in the ECO-reactor, Atomkernenergie 22, 1 (1973).

4. A. M. Weinberg and H. C. Schweinler, Theory of oscillating absorber in a chain reactor, Phys. Rev. 74, 851 (1948).

5. H. Van Dam, Neutron noise in boiling water reactors, Atomkernenergie 27, No. 1, 8 (1976).

6. I. Pazsit, Two group theory of noise in reflected reactors with application to vibrating absorbers, Annals of Nucl. Energy 5, 185 (1978).

7. A. Rohach, A polynomial nodal model using Legendre expansions, Ann. Nucl. Energy, Vol. 13, No. 2, pp 57-62 (1986)

8. A. Rohach, A Legendre polynomial nodal model for 2-D diffusion problems, Ann. Nucl. Energy, Vol. 13, No. 10, pp 549-558, (1986)

9. M. Feiz, Application of finite element nodal model to multigroup diffusion theory, Unpublished M.S. Theisis, Iowa State University (1983).

10. H. W. Graves, Jr. Nuclear Fuel Management. John Wiley & Sons, New York, New York, (1979).

11. M. Al-Ammar, Use of the Local-Global concept in detecting component vibration in reactors, Unpublished Ph.D. Dissertation, Iowa State University (1981).

12. T. B. Fowler, M. L. Tobias, and D. R. Vondy, EXTERMINATOR-2: A fortran IV code for solving multigroup neutron diffusion equations in two dimensions, ORNL-TM-4078, Oak Ridge National Laboratory (April 1967).

13. I. Pazsit and G. Th. Analytis, Theoretical investigation of the neutron noise diagnostics of two-dimensional control rod vibrations in a PWR, Annals of Nucl. Energy 7, 171 (1980).

14. J. Duderstadt and L. Hamilton, Nuclear Reactor Analysis, Wiley, New York (1976).

15. R. E. Uhrig, Measurment of reactor shutdown margin by noise analysis, Reactor Kinetics Control, (April 1964).

16. G. Kosaly and M. M. R. Williams, Point theory of the neutron noise induced by inlet temperature fluctuations and random mechanical vibrations, Atomkernenergie 18, 203 (1971).

17. I. Pazsit, Investigation of the space-dependent noise induced by a vibrating absorber, Atomkernenergie 30, 29 (1977).

18. G. Th. Analytis, A three-dimensional theoratical investigation of the Local and Global component of neutron noise in bare homogenous water moderated reactors and applications, Annals of Nuclear Energy 7:351 (1980).

19. S. J. Lee and R. W. Albrecht, Vibration-induced neutron fluctuations in a cylindrical two-group reactor, Transactions of the American Nuclear Society 39:953 (1981).

20. S. J. Lee and R. W. Albrecht, The use of neutronic fluctuations to locate a vibrating control rod in a pressurized water reactor model, Nuclear Science and Engineering 83:427 (1983).

21. I. Pazsit and O. Glockler, On the neutron noise diagnostics of pressurized water reactor control rod vibrations. 1. periodic vibrations, Nuclear Science and Engineering 85:167 (1983).

22. I. Pazsit and O. Glockler, On the neutron noise diagnostics of pressurized water reactor control rod vibrations II. Stochastic vibrations, Nuclear Science and Engineering 88:77 (1984).

23. L. R. Huang and R. A. Danofsky, A generalized model for predicting a neutron detector response to core parametric fluctuations, Transaction of the American Nuclear Society 34:831 (1980).

24. W. J. Hennessy, An investigation of the two-dimensional neutron noise field generated by a moving neutron absorber using the UTR-10 reactor, Unpublished M.S. Thesis, Iowa State University (1983).

25. M. Al-Ammar and R. A. Danofsky, Detection of component vibration in reactors based on the Local-Global interaction, Transaction of the American Nuclear Society 39:955 (1981).

26. R. J. Borland, Effects of neutron flux gradient and detector vibrator geometry on the Local-Global responses of the UTR-10 Reactor, Unpublished M.S. Thesis, Iowa State University (1982).

27. J. T. Sankoorikal, Vibration identification of reactor components by statistical analysis of neutron noise, Unpublished Ph.D. Dissertation, Iowa State University (1986).

28. P. M. Morse and H. Feshback, Methods of theoretical physics, McGraw-Hill Book Company, New York, (1953).

29. J. R. Lamarsh. Nuclear Reactor Theory. Addison-Wesley Publishing Company, New York, New York, (1966).

30. G. I. Bell and S. Glasston, Nuclear reactor theory, Van Nostrand Reinhold Company, New York, (1970).

31. R. L. Burden et al. Numerical Analysis. Prindle,Weber and Schmidt, Boston Massachusetts, July, (1981).

32. M. Benghanam, Enhanced convergence technique for a one dimensional nodal model, Unpublished M.S. Thesis, Iowa State University (1983).

33. Argonne Code Center: Benchmark problem book, American Nuclear Society, La Grange park, Ill. pp 368, June, (1977).

IX. ACKNOWLEDGEMENTS

The author wishes to acknowledge his gratitude and appreciation to his major professors Dr. R. A. Danofky and Dr. A. F. Rohach for the valuable suggestions, guidance and encouragement during the different phases of this research. The author wishes to express his indebtedness to the department of Nuclear Engineering for providing financial assistance. The author would also like to thank Dr. B. Spinrad for his valuable advice during the various stages of this research. Finally, the author is deeply grateful to his wife Naseem, for her encouragement and understanding through the years of study.